

A STABLE MIMETIC FINITE-DIFFERENCE METHOD FOR CONVECTION-DOMINATED DIFFUSION EQUATIONS *

JAMES H. ADLER[†], CASEY CAVANAUGH[‡], XIAOZHE HU[†], ANDY HUANG[§], AND NATHANIEL TRASK[¶]

Abstract. Convection-diffusion equations arise in a variety of applications such as particle transport, electromagnetics, and magnetohydrodynamics. Simulation of the convection-dominated regime for these problems, even with high-fidelity techniques, is particularly challenging due to the presence of sharp boundary layers and shocks causing jumps and discontinuities in the solution, and numerical issues such as loss of the maximum principle in the discretization. These complications cause instabilities, admitting large oscillations in the numerical solution when using traditional methods. Drawing connections to the simplex-averaged finite-element method (S. Wu and J. Xu, 2020), this paper develops a mimetic finite-difference (MFD) discretization using exponentially-averaged coefficients to overcome instability of the numerical solution as the diffusion coefficient approaches zero. The finite-element framework allows for transparent analysis of the MFD, such as proving well-posedness and deriving error estimates. Numerical tests are presented confirming the stability of the method and verifying the error estimates.

Key words. Convection-diffusion, mimetic-finite difference method, finite-element method, monotonicity, exponential fitting.

AMS subject classifications. 35M12, 65N06, 65N30

1. Introduction. Convection-diffusion equations, particularly describing phenomena in the convection-dominated regime, come in both scalar and vector forms, and have many important applications. In particular, the *scalar* convection-diffusion equation, for unknown u ,

$$(1.1) \quad \begin{aligned} -\operatorname{div}(\alpha \operatorname{grad} u + \beta u) + \gamma u &= f && \text{in } \Omega, \\ u &= 0 && \text{on } \partial\Omega, \end{aligned}$$

is commonly seen in particle transport [14, 31, 41, 45, 49, 57, 62]. Here, α and γ are real-valued scalar functions and β is a vector function representing various physical parameters. The *vector* convection-diffusion equations, which come in two forms,

$$(1.2) \quad \begin{aligned} \operatorname{curl}(\alpha \operatorname{curl} \mathbf{u} + \beta \times \mathbf{u}) + \gamma \mathbf{u} &= \mathbf{f} && \text{in } \Omega, \\ \mathbf{n} \times \mathbf{u} &= \mathbf{0} && \text{on } \partial\Omega, \end{aligned}$$

$$(1.3) \quad \begin{aligned} -\operatorname{grad}(\alpha \operatorname{div} \mathbf{u} + \beta \cdot \mathbf{u}) + \gamma \mathbf{u} &= \mathbf{f} && \text{in } \Omega, \\ \mathbf{u} \cdot \mathbf{n} &= 0 && \text{on } \partial\Omega, \end{aligned}$$

arise in electromagnetic applications such as magnetohydrodynamics [15, 35, 40, 55, 56], with β representing an externally applied field.

For this paper, we are interested in the convection-dominated case, where $|\alpha| \ll |\beta|$, as it poses difficulties in numerical simulations (see [50] for a survey). From

*Revision submitted to the editors May, 22 2023.

[†]Department of Mathematics, Tufts University, Medford, MA 02155 (james.adler@tufts.edu, xiaozhe.hu@tufts.edu).

[‡]Center for Computation and Technology, Louisiana State University, Baton Rouge, LA 70803 (Ccavanaugh@cct.lsu.edu)

[§]Radiation and Electrical Science, Sandia National Laboratories (ahuang@sandia.gov).

[¶]Center for Computing Research, Sandia National Laboratories (natrask@sandia.gov).

PDE theory [33], the convection-diffusion equation is elliptic; however, in the limiting case of $\alpha \rightarrow 0$, this is no longer true. As outlined in [50], this loss of ellipticity causes methods developed for the diffusion-dominated (elliptic) problem to fail in the limiting case, resulting in large numerical oscillations when solutions involve internal or boundary layers and shocks. One approach to restoring the stability is developing a *monotone* scheme for which a discrete maximum principle holds.

For the scalar convection-diffusion equation, (1.1), stabilized and monotone methods have been developed to avoid these common numerical difficulties. One choice is finite-difference or finite-volume schemes using upwinding [7, 8]. Additionally, there are a variety of finite-element (FE) schemes, like discontinuous Galerkin [5, 22, 39], streamline-upwind Petrov–Galerkin (SUPG) [24, 26], bubble function stabilized methods [17, 18, 23, 34], penalty methods [25, 27], and Petrov–Galerkin methods [30, 51] that all provide stabilized discretizations for the scalar equation (1.1). In [4], an $\mathbf{H}(\text{curl})$ -elliptic problem with discontinuous coefficients is considered using DG and auxiliary space preconditioners achieving scalable results. Additionally, while there is no explicit maximum principle for the convection-diffusion vector equations, there are a few approaches which provide a unifying framework for the general (both scalar and vector) convection-diffusion equation using Whitney forms [13] and k -forms [36, 37], which numerically demonstrate stability in the limiting regime.

The approach that we focus on here is exponential fitting [9, 19–21, 32, 42–44, 54, 63, 65]. In particular, for (1.1) we consider the edge-averaged finite-element method (EAFE) [65], which uses exponential shifting to recast the convection-diffusion problem as a modified Poisson equation. This approach has many advantages, such as a bilinear form to provide straightforward analysis of the scheme, and a provably monotone matrix formulation. Using Whitney forms and a discrete de Rham complex, the EAFE scheme was extended to the vector convection-diffusion equations, (1.2) and (1.3), using the simplex-averaged finite-element method (SAFE) [63]. Again, using exponential shifting with average integrals over the appropriate simplex, each convection-diffusion equation can be recast as a pure diffusion problem with a low-order term added to deal with the large nullspaces of the vector equations. This allows for implementation using exponentially-averaged coefficients in a standard FE approximation of a diffusion equation, and a clear avenue to develop the corresponding analysis and establish monotonicity. Furthermore, the SAFE method establishes a general framework for all three convection-diffusion equations, and ensures that the corresponding exponentially-shifted differential operators, called the flux operators, are structure-preserving in the continuous problem. However, while the SAFE flux operators satisfy a discrete de Rham complex before quadrature is introduced, the exact sequence does not hold in implementation unless the diffusion and convection coefficients are both constant.

The goal of this paper is to develop a general framework for a stable mimetic finite-difference (MFD) method for the convection-diffusion equation in both scalar and vector forms. There are many advantages to the MFD approach, including the ability to work with general polyhedral meshes, fast assembly of matrix systems, and the natural inheritance of a de Rham complex. Specifically for the convection-diffusion scheme, we show that the MFD method guarantees that the flux differential operators also satisfy a discrete de Rham sequence regardless of how any integrals are computed. Another major advantage of the stable MFD scheme, and of MFD more generally, is that it is related to discrete exterior calculus (DEC). As opposed to finite-element exterior calculus (FEEC), the DEC approach eliminates the need for mass matrices, which are tied to a specific mesh geometry and dimension. More

specifically, MFD guarantees structure-preserving operators which are scaled mesh incidence matrices. The incidence matrices more naturally extend to higher-order problems since they are not tied to any particular coordinate system, paving the way for connections to novel methods in machine learning. For instance, the MFD and DEC approach is advantageous to structure-preserving machine learning methods where a graph incidence matrix of a graph in \mathbb{R}^n is known and the appropriate metrics can be learned using a neural network [60]. Thus, the stable MFD scheme aids the development of structure-preserving machine learning methods for problems where standard approaches struggle due to the curse of dimensionality. Additionally, there are known connections between the MFD and traditional FE methods [1, 53] which can be applied to the convection-diffusion scheme. These connections provide a transparent approach to establishing well-posedness and error estimates in the FE setting for the MFD method. Finally, the MFD method yields a linear system resembling a scaled Laplacian from which monotonicity of the scalar convection-diffusion scheme is proven. This validates the stability of the scheme in the convection-dominated regime.

This paper is organized as follows. Section 2 defines notation and briefly presents the standard FE and MFD methods. In Section 3, we introduce the key features of the SAFE method and the corresponding mimetic approach. We also present the full discretized scheme, suggest quadrature rules, and discuss numerical stability in the implementation. Connections to the finite-element method are given in Section 4, along with an analysis of the scheme including well-posedness results and error estimates. Numerical results are presented in Section 5 and, finally, Section 6 summarizes the conclusions and presents ideas for future work.

2. Preliminaries. In this section, we introduce notation used in the paper and briefly recall the MFD method. For ease of the analysis, we assume $\Omega \in \mathbb{R}^3$ is a bounded polyhedron domain. However, all the results hold for the two-dimensional case with minor modifications, and the illustrations and numerical results are performed on \mathbb{R}^2 for simplicity. In the rest of this paper, for an open subset $\omega \in \mathbb{R}^d$, we use the standard notation for Sobolev spaces, $W^{\ell,p}(\omega)$, $0 \leq \ell < \infty$, $1 \leq p \leq \infty$, and their associated norm, $\|\cdot\|_{\ell,p,\omega}$, and semi-norm, $|\cdot|_{\ell,p,\omega}$. For $p = 2$, we use the standard notation, $H^\ell(\omega) := W^{\ell,2}(\omega)$ with norm $\|\cdot\|_{\ell,\omega}$ and semi-norm $|\cdot|_{\ell,\omega}$. Furthermore, for $\ell = 0$, $H^0(\omega)$ coincides with the standard $L^2(\omega)$ space with inner product $\langle \cdot, \cdot \rangle_\omega$ and norm $\|\cdot\|_\omega$. Finally, when the context is clear, we omit ω in the notation, especially when $\omega = \Omega$.

2.1. The Finite-Element Method. Let the Sobolev space on Ω associated with differential operator, \mathfrak{D}^k , $k = 0, 1, 2$, be given by,

$$H(\mathfrak{D}^k) := \{u \mid u \in L^2(\Omega), \mathfrak{D}^k u \in L^2(\Omega)\},$$

with norm $\|\cdot\|_{H(\mathfrak{D}^k)}$, semi-norm $|\cdot|_{H(\mathfrak{D}^k)}$, and inner product $\langle \cdot, \cdot \rangle_{H(\mathfrak{D}^k)}$. Here, $\mathfrak{D}^0 = \text{grad}$, $\mathfrak{D}^1 = \text{curl}$, $\mathfrak{D}^2 = \text{div}$, and we have the following de Rham sequence,

$$(2.1) \quad H(\text{grad}) \xrightarrow{\text{grad}} \mathbf{H}(\text{curl}) \xrightarrow{\text{curl}} \mathbf{H}(\text{div}) \xrightarrow{\text{div}} L^2.$$

Note that we use boldface letters for the vector-valued functions and their corresponding function spaces. To make the notation consistent, we define $H(\mathfrak{D}^3) := L^2(\Omega)$, and as a result we have $\|\cdot\|_{H(\mathfrak{D}^0)} = \|\cdot\|_1$ and $\|\cdot\|_{H(\mathfrak{D}^3)} = \|\cdot\|$, for example.

Given a simplicial mesh, \mathcal{T} , of the domain Ω , we consider the lowest-order conforming FE spaces for $H(\mathfrak{D}^k)$, denoted by $H_h(\mathfrak{D}^k)$, $k = 0, 1, 2$. On the mesh, we

have k -simplices, denoted by s^0 (vertices), s^1 (edges), s^2 (faces), and s^3 (volumes), where s_i^k denotes the i -th k -simplex in the mesh enumeration. Next, define the corresponding degrees of freedom (DoFs) $\{\eta_i^k\}_{s_i^k \in \mathcal{T}}$ and FE basis functions $\{\lambda_i^k\}_{s_i^k \in \mathcal{T}}$, for each space $H(\mathfrak{D}^k)$, $k = 0, 1, 2$. In addition, a piecewise constant FE space is used for $L^2(\Omega)$ and is denoted as L_h^2 (or $H_h(\mathfrak{D}^3)$) with DoFs $\{\eta_i^3\}$ and basis functions $\{\lambda_i^3\}$. Specifically, for a vertex i with coordinate \mathbf{x}_i , edge e_i with unit tangent \mathbf{t}_i and length $|e_i|$, face f_i with unit normal \mathbf{n}_i and area $|f_i|$, and simplex T_i with volume $|T_i|$, we have the DoFs,

$$\begin{aligned}\eta_i^0(u) &= u(\mathbf{x}_i), \\ \boldsymbol{\eta}_i^1(\mathbf{u}) &= \frac{1}{|e_i|} \int_{e_i} (\mathbf{u} \cdot \mathbf{t}_i) ds, \\ \boldsymbol{\eta}_i^2(\mathbf{u}) &= \frac{1}{|f_i|} \int_{f_i} (\mathbf{u} \cdot \mathbf{n}_i) dA, \\ \eta_i^3(u) &= \frac{1}{|T_i|} \int_{T_i} u dV.\end{aligned}$$

Since (1.1)–(1.3) are given with Dirichlet boundary conditions, the following FE spaces with boundary conditions are considered,

$$\begin{aligned}H_{h,0}(\text{grad}) &:= \{u \mid u \in H_h(\text{grad}), u|_{\partial\Omega} = 0\}, \\ \mathbf{H}_{h,0}(\text{curl}) &:= \{\mathbf{u} \mid \mathbf{u} \in \mathbf{H}_h(\text{curl}), \mathbf{n} \times \mathbf{u}|_{\partial\Omega} = 0\}, \\ \mathbf{H}_{h,0}(\text{div}) &:= \{\mathbf{u} \mid \mathbf{u} \in \mathbf{H}_h(\text{div}), \mathbf{u} \cdot \mathbf{n}|_{\partial\Omega} = 0\}.\end{aligned}$$

It is well-known from finite-element exterior calculus (FEEC) [2, 3, 38] that the corresponding function spaces for these choices of elements satisfy a de Rham sequence,

$$(2.2) \quad H_{h,0}(\text{grad}) \xrightarrow{\text{grad}} \mathbf{H}_{h,0}(\text{curl}) \xrightarrow{\text{curl}} \mathbf{H}_{h,0}(\text{div}) \xrightarrow{\text{div}} L_h^2.$$

Next, we introduce the corresponding discrete differential operators. The FE gradient, G_{FE} , curl, K_{FE} , and divergence, D_{FE} , operators are expressed in terms of the basis functions and DoFs,

$$\begin{aligned}(G_{\text{FE}})_{ij} &:= \boldsymbol{\eta}_i^1(\text{grad } \lambda_j^0) = \frac{1}{|e_i|} \int_{e_i} \text{grad } \lambda_j^0 \cdot \mathbf{t}_i ds, \\ (K_{\text{FE}})_{ij} &:= \boldsymbol{\eta}_i^2(\text{curl } \boldsymbol{\lambda}_j^1) = \frac{1}{|f_i|} \int_{f_i} \text{curl } \boldsymbol{\lambda}_j^1 \cdot \mathbf{n}_i dA, \\ (D_{\text{FE}})_{ij} &:= \eta_i^3(\text{div } \boldsymbol{\lambda}_j^2) = \frac{1}{|T_i|} \int_{T_i} \text{div } \boldsymbol{\lambda}_j^2 dV.\end{aligned}$$

By direct calculation, we have $K_{\text{FE}}G_{\text{FE}} = 0$ and $D_{\text{FE}}K_{\text{FE}} = 0$ which verifies properties of (2.2).

Finally, we introduce the usual canonical interpolation operator, which plays an essential role in drawing the connections between FEM and MFD schemes,

$$(2.3) \quad \Pi^k v = \sum_{s_i^k \in \mathcal{T}} \eta_i^k(v) \lambda_i^k, \quad \forall v \in H(\mathfrak{D}^k).$$

We also define notation for the average integral,

$$\int_{\mathcal{S}} f(\mathbf{x}) d\mathbf{x} := \frac{1}{|\mathcal{S}|} \int_{\mathcal{S}} f(\mathbf{x}) d\mathbf{x},$$

where \mathcal{S} denotes the region of the integration.

2.2. The Mimetic Finite-Difference Method. We next introduce the notation and differential operators for MFD. The foundation of the MFD method is a dual mesh configuration. The primal mesh is a Delaunay triangulation in 2 or 3 dimensions, with corresponding dual Voronoi polygonal or polyhedral mesh. Note that the finite-element mesh, \mathcal{T} defined above, corresponds to the primal Delaunay mesh defined here, but we change the notation slightly to more clearly describe the connection between the primal and dual meshes in the finite-difference setting.

Let N_D denote the number of Delaunay nodes \mathbf{x}_i^D . An edge connecting nodes \mathbf{x}_i^D and \mathbf{x}_j^D is given by \mathbf{e}_{ij}^D with unit tangent vector \mathbf{t}_{ij}^D pointing from vertex of lower index to vertex of higher index. The edge tangent vector (non-unit) is given by $\mathbf{T}_{ij}^D = \mathbf{t}_{ij}^D |\mathbf{e}_{ij}^D|$. A Delaunay element is given by D_k with boundary set ∂D_k . The set of indices of the elements that share a boundary with D_k is given by $\mathcal{N}_k^D := \{m \mid \partial D_k \cap \partial D_m \neq \emptyset, m = 1, \dots, N_D\}$. The shared boundary element (a face in 3D or edge in 2D) is given by ∂D_{km} which has an associated unit normal vector \mathbf{n}_{km}^D , which points outward from element D_k . Similarly, on the Voronoi mesh we define number of nodes N_V , nodes \mathbf{x}_k^V , edge \mathbf{e}_{km}^V with unit tangent \mathbf{t}_{km}^V , element V_i , boundary set ∂V_i , neighbor set \mathcal{N}_i^V , and boundary element ∂V_{ij} with outward unit normal \mathbf{n}_{ij}^V .

The MFD dual mesh configuration presents many useful geometric relationships. First, there are one-to-one relationships between nodes on one mesh and elements on the other. In particular, each Voronoi vertex \mathbf{x}_k^V is the circumcenter of the Delaunay element D_k , and each Voronoi element V_i is the set of points in the domain that lies closest to Delaunay point \mathbf{x}_i^D , $V_i := \{\mathbf{x} \in \Omega \mid |\mathbf{x} - \mathbf{x}_i^D| \leq |\mathbf{x} - \mathbf{x}_j^D|, j = 1, \dots, N_D, j \neq i\}$. Another correspondence is between edges on one mesh and faces on the other. Delaunay edge \mathbf{e}_{ij}^D and Voronoi face ∂V_{ij} are orthogonal such that $\mathbf{t}_{ij}^D \cdot \mathbf{n}_{ij}^V = \pm 1$. Analogously, we have that $\mathbf{t}_{km}^V \cdot \mathbf{n}_{km}^D = \pm 1$ resulting in Voronoi edge \mathbf{e}_{km}^V and Delaunay face ∂D_{km} also being orthogonal. These relationships are demonstrated in Figure 1. Note that the dual grid is not required to be a Voronoi diagram, though the construction of an alternate dual grid should maintain the same properties: the one-to-one relationships previously mentioned, and orthogonality of edges on one mesh with faces on the other.

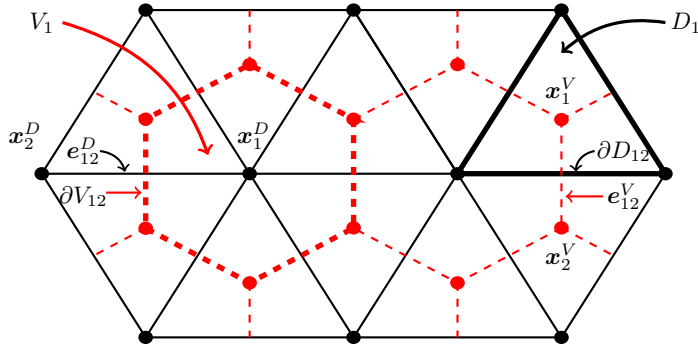


Fig. 1: Two-dimensional MFD mesh with Voronoi element V_1 corresponding to Delaunay point \mathbf{x}_1^D , and Delaunay element D_1 corresponding to Voronoi point \mathbf{x}_1^V . Delaunay edge \mathbf{e}_{12}^D is orthogonal to Voronoi face (edge) ∂V_{12} , and similarly, Voronoi edge \mathbf{e}_{12}^V is orthogonal to Delaunay face (edge) ∂D_{12} .

As in [12, 61], we proceed by defining scalar and vector function spaces on the two meshes, and the usual discrete differential operators. The space of scalar functions will be approximated as piecewise constants on the nodes of the mesh as follows:

$$\begin{aligned} H_D &:= \{u(\mathbf{x}) \mid u(\mathbf{x}) = u_i^D := u(\mathbf{x}_i^D), \forall \mathbf{x} \in V_i, i = 1, \dots, N_D\}, \\ H_V &:= \{u(\mathbf{x}) \mid u(\mathbf{x}) = u_k^V := u(\mathbf{x}_k^V), \forall \mathbf{x} \in D_k, k = 1, \dots, N_V\}. \end{aligned}$$

Vector functions, $\mathbf{u}(\mathbf{x})$, on the other hand, are approximated along the mesh edges. The Delaunay space of discrete vector functions, \mathbf{H}_D , is formed by taking projections onto edges and evaluating at the intersection of the Delaunay edge and corresponding Voronoi interface. The space of Voronoi vector functions, \mathbf{H}_V , is defined analogously:

$$\begin{aligned} \mathbf{H}_D &:= \{\mathbf{u}(\mathbf{x}) \mid \mathbf{u}(\mathbf{x}) = u_{ij}^D := (\mathbf{u} \cdot \mathbf{t}_{ij}^D)(\mathbf{x}_{ij}^D), \mathbf{x}_{ij}^D = \mathbf{e}_{ij}^D \cap \partial V_{ij}\}, \\ \mathbf{H}_V &:= \{\mathbf{u}(\mathbf{x}) \mid \mathbf{u}(\mathbf{x}) = u_{km}^V := (\mathbf{u} \cdot \mathbf{t}_{km}^V)(\mathbf{x}_{km}^V), \mathbf{x}_{km}^V = \mathbf{e}_{km}^V \cap \partial D_{km}\}. \end{aligned}$$

The usual differential operators grad, curl, div are well-known and easily derived from discrete versions of the calculus theorems [12, 48, 61]. On the Delaunay mesh, we have $\text{grad}_D u : H_D \rightarrow \mathbf{H}_D$ on edge \mathbf{e}_{ij}^D ,

$$(2.4) \quad (\text{grad}_D u)_{ij}^D = \frac{u_j^D - u_i^D}{|\mathbf{e}_{ij}^D|} \zeta(i, j),$$

where ζ is an orientation constant that $\zeta(i, j) = 1$ if $j > i$ and, otherwise, $\zeta = -1$. We also have $\text{curl}_D u : \mathbf{H}_D \rightarrow \mathbf{H}_V$, measuring the rotation on Delaunay face ∂D_{km} ,

$$(2.5) \quad (\text{curl}_D u)_{km}^V = \frac{(\mathbf{t}_{km}^V \cdot \mathbf{n}_{km}^D)}{|\partial D_{km}|} \sum_{\mathbf{e}_{ij}^D \in \partial D_{km}} u_{ij}^D |\mathbf{e}_{ij}^D| \chi(\mathbf{n}_{km}^D, \mathbf{t}_{ij}^D),$$

where the constant χ enforces the direction of rotation, i.e., $\chi(\mathbf{n}_{km}^D, \mathbf{t}_{ij}^D) = 1$ if \mathbf{t}_{ij}^D is positively oriented and, otherwise, $\chi(\mathbf{n}_{km}^D, \mathbf{t}_{ij}^D) = -1$. In addition, we have the Voronoi divergence $\text{div}_V u : \mathbf{H}_V \rightarrow H_V$, corresponding to the outward flux of D_k ,

$$(2.6) \quad (\text{div}_V u)_k^V = \frac{1}{|D_k|} \sum_{m \in \mathcal{N}_k^D} |\partial D_{km}| u_{km}^V (\mathbf{n}_{km}^D \cdot \mathbf{t}_{km}^V).$$

The Voronoi mesh operators grad_V , curl_V , and Delaunay div_D are defined in a similar fashion. To write the operators in matrix form, we define the Delaunay edge-vertex signed incidence matrix, $\mathcal{G} \in \mathbb{R}^{M_D \times N_D}$, the Voronoi edge-vertex signed incidence matrix, $\mathcal{G}_V \in \mathbb{R}^{M_V \times N_V}$, and the Delaunay face-edge signed incidence matrix, $\mathcal{K} \in \mathbb{R}^{M_V \times M_D}$ where M_V is the number of Voronoi edges and M_D the number of Delaunay edges. Assuming a pre-determined orientation of the edges and faces, the nonzero entries of \mathcal{G} , \mathcal{G}_V , and \mathcal{K} are either 1 or -1 and capture the action of the operators. To scale appropriately, define the following diagonal matrices encoded with metric information on the meshes:

$$\begin{aligned} \mathcal{D}_{e^D} &= \text{diag}(|\mathbf{e}_{ij}^D|), & \mathcal{D}_{\partial D} &= \text{diag}(|\partial D_{km}|), & \mathcal{D}_D &= \text{diag}(|D_k|), \\ \mathcal{D}_{e^V} &= \text{diag}(|\mathbf{e}_{km}^V|), & \mathcal{D}_{\partial V} &= \text{diag}(|\partial V_{ij}|), & \mathcal{D}_V &= \text{diag}(|V_i|). \end{aligned}$$

Thus,

$$\begin{aligned} \text{grad}_D &:= \mathcal{D}_{e^D}^{-1} \mathcal{G}, & \text{div}_D &:= \mathcal{D}_V^{-1} \mathcal{G}^T \mathcal{D}_{\partial V}, & \text{curl}_D &:= \mathcal{D}_{\partial D}^{-1} \mathcal{K} \mathcal{D}_{e^D}, \\ \text{grad}_V &:= \mathcal{D}_{e^V}^{-1} \mathcal{G}_V, & \text{div}_V &:= \mathcal{D}_D^{-1} \mathcal{G}_V^T \mathcal{D}_{\partial D}, & \text{curl}_V &:= \mathcal{D}_{\partial V}^{-1} \mathcal{K}^T \mathcal{D}_{e^V}. \end{aligned}$$

A significant advantage of the mimetic differential operators is that they are structure-preserving, meaning that standard properties are preserved: $\text{curl}_D \text{grad}_D = 0$, $\text{curl}_V \text{grad}_V = 0$, $\text{div}_V \text{curl}_D = 0$, and $\text{div}_D \text{curl}_V = 0$ [12, 48, 61]. In essence, this means that the operators satisfy two exact sequences,

$$(2.7) \quad H_D \xrightarrow{\text{grad}_D} \mathbf{H}_D \xrightarrow{\text{curl}_D} \mathbf{H}_V \xrightarrow{\text{div}_V} H_V,$$

$$(2.8) \quad H_V \xrightarrow{\text{grad}_V} \mathbf{H}_V \xrightarrow{\text{curl}_V} \mathbf{H}_D \xrightarrow{\text{div}_D} H_D.$$

3. The MFD Method for the Convection Diffusion Problems. In this section, we introduce the proposed MFD scheme, and present the full stable discretization for the convection-diffusion problems, along with some implementation details. First, though, we review the key definitions and features of the SAFE method [63], which our approach is based on.

3.1. Shifted Flux Operators. The SAFE framework relies on exponential shifting of the usual grad, curl, and div operators to reformulate the convection-diffusion equation as a diffusion problem with exponential coefficients. The goal is to preserve the de Rham complex (2.1) with the new, shifted operators.

To start, define $\boldsymbol{\theta} = \boldsymbol{\beta}/\alpha$ as the ratio of convection to diffusion parameters, and introduce a potential function, φ , such that

$$(3.1) \quad \boldsymbol{\theta} = \text{grad } \varphi.$$

Then, the shifted flux operators are obtained as follows:

$$(3.2) \quad J^0 u = \text{grad } u + \boldsymbol{\theta} u = e^{-\varphi} \text{grad } (e^\varphi u),$$

$$(3.3) \quad J^1 \mathbf{u} = \text{curl } \mathbf{u} + \boldsymbol{\theta} \times \mathbf{u} = e^{-\varphi} \text{curl } (e^\varphi \mathbf{u}),$$

$$(3.4) \quad J^2 \mathbf{u} = \text{div } \mathbf{u} + \boldsymbol{\theta} \cdot \mathbf{u} = e^{-\varphi} \text{div } (e^\varphi \mathbf{u}).$$

This shifting can be thought of as an exponential transform on the function u , applying the derivative, and transforming back to the original space. Using this formulation, it is easily verified that,

$$J^1 \circ J^0 u = e^{-\varphi} \text{curl } (e^\varphi e^{-\varphi} \text{grad } (e^\varphi u)) = e^{-\varphi} \text{curl } (\text{grad } (e^\varphi u)) = \mathbf{0},$$

$$J^2 \circ J^1 \mathbf{u} = e^{-\varphi} \text{div } (e^\varphi e^{-\varphi} \text{curl } (e^\varphi \mathbf{u})) = e^{-\varphi} \text{div } (\text{curl } (e^\varphi \mathbf{u})) = 0.$$

Therefore, the flux operators J^0 , J^1 , and J^2 correspond to shifted grad, curl, and div operators, respectively, and admit the desired de Rham exact sequence,

$$(3.5) \quad H(\text{grad}) \xrightarrow{J^0} \mathbf{H}(\text{curl}) \xrightarrow{J^1} \mathbf{H}(\text{div}) \xrightarrow{J^2} L^2.$$

The benefit of this approach is that the convection term is built into the shifted differential operator. Thus, the convection-diffusion equations (1.1)–(1.3) are re-written as modified diffusion problems:

$$(3.6) \quad \begin{aligned} -\text{div } (\alpha J^0 u) + \gamma u &= f & \text{in } \Omega, \\ u &= 0 & \text{on } \partial\Omega; \end{aligned}$$

$$(3.7) \quad \begin{aligned} \operatorname{curl}(\alpha J^1 \mathbf{u}) + \gamma \mathbf{u} &= \mathbf{f} & \text{in } \Omega, \\ \mathbf{n} \times \mathbf{u} &= \mathbf{0} & \text{on } \partial\Omega; \end{aligned}$$

$$(3.8) \quad \begin{aligned} -\operatorname{grad}(\alpha J^2 \mathbf{u}) + \gamma \mathbf{u} &= \mathbf{f} & \text{in } \Omega, \\ \mathbf{u} \cdot \mathbf{n} &= 0 & \text{on } \partial\Omega. \end{aligned}$$

Remark 3.1. This framework relies on (3.1), the ability to re-write the ratio of the convection to diffusion parameters in terms of a potential function. Although this can be done for a wide range of functions, for arbitrary function $\boldsymbol{\theta}(\mathbf{x})$, we should not expect this to always be possible. One solution to handle this case would be to take a piecewise constant approximation of $\boldsymbol{\theta}$ on the mesh, as is done in [63]. However, this may destroy the de Rham complex (3.5). An alternative option would be to decompose $\boldsymbol{\theta}$ using a Helmholtz decomposition, i.e., $\boldsymbol{\theta} = \operatorname{grad} \varphi + \operatorname{curl} \boldsymbol{\psi}$, and build the flux operators using the $\operatorname{grad} \varphi$ part. Section 5.4 provides numerical examples for the scalar convection-diffusion equation, where the convection coefficient is written in terms of this Helmholtz decomposition. In many practical applications, though, such as the drift-diffusion equations, the convection coefficient is naturally given as the gradient of a potential function.

3.2. Discrete MFD flux operators. Next, we consider a discretization of the shifted flux operators (3.2)–(3.4) using MFD. In particular, we choose to discretize J^0 and J^1 on the Delaunay mesh, and J^2 on the Voronoi mesh to recover something resembling the MFD de Rham complex (2.7).

Starting with the J^0 operator, rearrange (3.2) slightly and integrate over a Delaunay edge e_{ij}^D , to obtain

$$\int_{e_{ij}^D} e^\varphi J^0 u \cdot \mathbf{t}_{ij}^D \, ds = \int_{e_{ij}^D} \operatorname{grad}(e^\varphi u) \cdot \mathbf{t}_{ij}^D \, ds.$$

The right-hand side can be directly integrated using the fundamental theorem of calculus. On the left-hand side, we use the basic idea of an MFD method and approximate $J^0 u \cdot \mathbf{t}_{ij}^D$ by a constant on the edge, denoted by $(\mathcal{J}_D^0 u)_{ij}^D$. Thus, denoting $\varphi_i = \varphi(\mathbf{x}_i^D)$, the discrete MFD flux operator, $\mathcal{J}_D^0 : H_D \rightarrow \mathbf{H}_D$, is defined as

$$(3.9) \quad (\mathcal{J}_D^0 u)_{ij}^D := \frac{e^{\varphi_j} u_j^D - e^{\varphi_i} u_i^D}{|e_{ij}^D| \int_{e_{ij}^D} e^\varphi \, ds} \zeta(i, j).$$

Next, for J^1 , rearrange (3.3) and integrate over a Delaunay face to obtain

$$\int_{\partial D_{km}} e^\varphi J^1 \mathbf{u} \cdot \mathbf{n}_{km}^D \, dA = \int_{\partial D_{km}} \operatorname{curl}(e^\varphi \mathbf{u}) \cdot \mathbf{n}_{km}^D \, dA.$$

Approximating $J^1 \mathbf{u} \cdot \mathbf{n}_{km}^D$ with constant $(\mathcal{J}_D^1 u)_{km}^V$ on the face and directly evaluating the right-hand side using Stokes' Theorem, we define the following discrete MFD flux operator $\mathcal{J}_D^1 : \mathbf{H}_D \rightarrow \mathbf{H}_V$,

$$(3.10) \quad (\mathcal{J}_D^1 u)_{km}^V := (\mathbf{n}_{km}^D, \mathbf{t}_{ij}^D) \sum_{e_{ij}^D \in \partial D_{km}} \frac{|e_{ij}^D| \int_{e_{ij}^D} e^\varphi \, ds}{|\partial D_{km}| \int_{\partial D_{km}} e^\varphi \, dA} u_{ij}^D \chi(\mathbf{n}_{km}^D, \mathbf{t}_{ij}^D).$$

Following the same procedure for approximating J^2 , rearrange (3.4) and integrate over a Delaunay element to obtain

$$\int_{D_k} e^\varphi J^2 \mathbf{u} \, dV = \int_{D_k} \operatorname{div} (e^\varphi \mathbf{u}) \, dV.$$

Here, the right-hand side can be directly evaluated using the divergence theorem, and a constant approximation of $J^2 \mathbf{u}$ on the element D_k yields the MFD flux operator $\mathcal{J}_V^2 : \mathbf{H}_V \rightarrow H_V$,

$$(3.11) \quad (\mathcal{J}_V^2 u)_k^V := \sum_{m \in \mathcal{N}_k^D} \frac{|\partial D_{km}| \int_{\partial D_{km}} e^\varphi \, dA}{|D_k| \int_{D_k} e^\varphi \, dV} u_{km}^V (\mathbf{n}_{km}^D \cdot \mathbf{t}_{km}^V).$$

All three discrete MFD flux operators, \mathcal{J}_D^0 , \mathcal{J}_D^1 , and \mathcal{J}_V^2 , have the same form as the usual MFD grad_D (2.4), curl_D (2.5) and div_V (2.6). The only difference is the scaling, which reflects the exponential shifting seen as the average exponential integrals in the coefficients. Therefore, to write the discrete MFD flux operators in matrix form, we use the incidence matrices \mathcal{G} and \mathcal{K} , along with the following diagonal matrices for the average exponential integrals,

$$(3.12) \quad \begin{aligned} E_{\mathbf{x}^D} &= \operatorname{diag} \left(e^{\varphi(\mathbf{x}_i^D)} \right), \quad E_{\mathbf{e}^D} = \operatorname{diag} \left(\int_{\mathbf{e}_{ij}^D} e^\varphi \, ds \right), \\ E_{\partial D} &= \operatorname{diag} \left(\int_{\partial D_{km}} e^\varphi \, dA \right), \quad E_D = \operatorname{diag} \left(\int_{D_k} e^\varphi \, dV \right). \end{aligned}$$

Thus, the matrix form of the discrete flux operators is given by,

$$(3.13) \quad \mathcal{J}_D^0 := E_{\mathbf{e}^D}^{-1} \mathcal{D}_{\mathbf{e}^D}^{-1} \mathcal{G} E_{\mathbf{x}^D} = E_{\mathbf{e}^D}^{-1} \operatorname{grad}_D E_{\mathbf{x}^D},$$

$$(3.14) \quad \mathcal{J}_D^1 := E_{\partial D}^{-1} \mathcal{D}_{\partial D}^{-1} \mathcal{K} \mathcal{D}_{\mathbf{e}^D} E_{\mathbf{e}^D} = E_{\partial D}^{-1} \operatorname{curl}_D E_{\mathbf{e}^D},$$

$$(3.15) \quad \mathcal{J}_V^2 := E_D^{-1} \mathcal{D}_D^{-1} \mathcal{G}_V^T \mathcal{D}_{\partial D} E_{\partial D} = E_D^{-1} \operatorname{div}_V E_{\partial D}.$$

From this, it is easy to show that $\mathcal{J}_D^1 \mathcal{J}_D^0 = 0$ and $\mathcal{J}_V^2 \mathcal{J}_D^1 = 0$, and that the MFD exact sequence is preserved,

$$H_D \xrightarrow{\mathcal{J}_D^0} \mathbf{H}_D \xrightarrow{\mathcal{J}_D^1} \mathbf{H}_V \xrightarrow{\mathcal{J}_V^2} H_V.$$

Note that this holds regardless of how the exponential integrals are computed, so long as the same approach (i.e., quadrature rule) is used consistently across the three discrete MFD flux operators.

Remark 3.2. The above sequence corresponds to the MFD sequence (2.7), which relates to solving (3.6)–(3.8) in primal form. The derivation of the flux operators in Section 3.2 will give the flux operators corresponding to the second MFD exact sequence (2.8) by simply swapping primal mesh quantities (\mathbf{x}_i^D , \mathbf{e}_{ij}^D , ∂D_{km} , and D_k) for the corresponding dual mesh quantity (\mathbf{x}_k^V , \mathbf{e}_{km}^V , ∂V_{ij} , and V_i , respectively), and vice versa.

3.3. Full MFD Scheme and Implementation. With the flux operators defined in the MFD setting (3.13)–(3.15), the fully discretized convection-diffusion equations (3.6)–(3.8) can be written: Find $u_D \in H_D$ such that,

$$(3.16) \quad \begin{aligned} \operatorname{div}_D (\mathcal{D}_{\alpha, \mathbf{e}^D} \mathcal{J}_D^0 u_D) + \mathcal{D}_{\gamma, \mathbf{x}^D} u_D &= f_D \quad \text{in } \Omega, \\ u_D &= 0 \quad \text{on } \partial\Omega; \end{aligned}$$

find $\mathbf{u}_D \in \mathbf{H}_D$ such that,

$$(3.17) \quad \begin{aligned} \operatorname{curl}_V (\mathcal{D}_{\alpha, e^V} \mathcal{J}_D^1 \mathbf{u}_D) + \mathcal{D}_{\gamma, e^D} \mathbf{u}_D &= \mathbf{f}_D \quad \text{in } \Omega, \\ \mathbf{u}_D &= 0 \quad \text{on } \partial\Omega; \end{aligned}$$

and find $\mathbf{u}_V \in \mathbf{H}_V$ such that

$$(3.18) \quad \begin{aligned} \operatorname{grad}_V (\mathcal{D}_{\alpha, \mathbf{x}^V} \mathcal{J}_V^2 \mathbf{u}_V) + \mathcal{D}_{\gamma, e^V} \mathbf{u}_V &= \mathbf{f}_V \quad \text{in } \Omega, \\ \mathbf{u}_V &= 0 \quad \text{on } \partial\Omega, \end{aligned}$$

where $\mathcal{D}_{\alpha, e^D}$, $\mathcal{D}_{\alpha, e^V}$, and $\mathcal{D}_{\alpha, \mathbf{x}^V}$ are diagonal matrices of suitable piecewise constant approximations of the average value of the diffusion coefficient, $\alpha(\mathbf{x})$, on the Delaunay edges, Voronoi edges, and Voronoi nodes, respectively. Similarly, $\mathcal{D}_{\gamma, \mathbf{x}^D}$, $\mathcal{D}_{\gamma, e^D}$, and $\mathcal{D}_{\gamma, e^V}$ are diagonal matrices of suitable piecewise constant approximations of the average values of the coefficient $\gamma(\mathbf{x})$ on the Delaunay nodes, Delaunay edges, and Voronoi edges, respectively. Additionally, f_D , \mathbf{f}_D , and \mathbf{f}_V are all suitable discretizations of the continuous right-hand sides of (1.1)–(1.3). In particular,

(3.19)

$$\mathcal{D}_{\alpha, e^D} = \operatorname{diag} \left(\int_{e_{ij}^D} \alpha ds \right), \quad \mathcal{D}_{\alpha, e^V} = \operatorname{diag} \left(\int_{\partial D_{km}} \alpha dA \right), \quad \mathcal{D}_{\alpha, \mathbf{x}^V} = \operatorname{diag} \left(\int_{D_k} \alpha dV \right),$$

(3.20)

$$\mathcal{D}_{\gamma, \mathbf{x}^D} = \operatorname{diag} (\gamma(\mathbf{x}_i^D)), \quad \mathcal{D}_{\gamma, e^D} = \operatorname{diag} \left(\int_{e_{ij}^D} \gamma ds \right), \quad \mathcal{D}_{\gamma, e^V} = \operatorname{diag} \left(\int_{\partial D_{km}} \gamma dA \right).$$

(3.21)

$$f_D = \operatorname{vec} (f(\mathbf{x}_i^D)), \quad \mathbf{f}_D = \operatorname{vec} \left(\int_{e_{ij}^D} \mathbf{f} ds \right), \quad \mathbf{f}_V = \operatorname{vec} \left(\int_{\partial D_{km}} \mathbf{f} dA \right).$$

3.3.1. Quadrature Rules. The discrete MFD flux operators (3.9)–(3.11) are defined with the exponential integrals computed exactly. In practice, this is intractable and a quadrature rule is required. Since we have an exponential function in the integrand, a simple numerical integration rule might not guarantee the desired accuracy. Therefore, we consider quadrature rules that are exact when $\boldsymbol{\theta}$ is a constant on the integral domain, which is equivalent to assuming a linear potential function φ . Full derivations of these schemes can be found in [29], and we state the results here.

For $E_{e^D} = \operatorname{diag} \left(\int_{e_{ij}^D} e^\varphi ds \right)$, we use the following edge quadrature rule,

$$(3.22) \quad \int_{e_{ij}^D} e^\varphi ds \approx \frac{e^{\varphi_j} - e^{\varphi_i}}{(\boldsymbol{\theta}_{ij} \cdot \mathbf{T}_{ij}^D)},$$

where $\boldsymbol{\theta}_{ij}$ is a constant approximation of $\boldsymbol{\theta}$ on the edge e_{ij}^D and $\mathbf{T}_{ij}^D = \mathbf{t}_{ij}^D |e_{ij}^D|$. It is easy to verify that this quadrature rule is exact if $\boldsymbol{\theta}$ is constant on the edge e_{ij}^D . For $E_{\partial D} = \operatorname{diag} \left(\int_{\partial D_{pm}} e^\varphi dA \right)$, let $\mathbf{x}_i^D, \mathbf{x}_j^D, \mathbf{x}_k^D$ be the indices of face ∂D_{pm} where it is assumed that $i < j < k$. Then, we obtain the following face quadrature rule,

(3.23)

$$\int_{\partial D_{pm}} e^\varphi dA \approx 2 \left(\frac{e^{\varphi_i}}{(\boldsymbol{\theta}_{ij} \cdot \mathbf{T}_{ij}^D)(\boldsymbol{\theta}_{ik} \cdot \mathbf{T}_{ik}^D)} - \frac{e^{\varphi_j}}{(\boldsymbol{\theta}_{ij} \cdot \mathbf{T}_{ij}^D)(\boldsymbol{\theta}_{jk} \cdot \mathbf{T}_{jk}^D)} + \frac{e^{\varphi_k}}{(\boldsymbol{\theta}_{jk} \cdot \mathbf{T}_{jk}^D)(\boldsymbol{\theta}_{ik} \cdot \mathbf{T}_{ik}^D)} \right),$$

which is exact if $\boldsymbol{\theta}$ is a constant on the face ∂D_{pm} . Lastly, for $E_D = \text{diag} \left(\int_{D_p} e^\varphi dV \right)$, let $\boldsymbol{x}_i^D, \boldsymbol{x}_j^D, \boldsymbol{x}_k^D, \boldsymbol{x}_\ell^D$ be the indices of element ∂D_p where it is assumed that $i < j < k < \ell$. Then, we have the following element quadrature rule,

$$(3.24) \quad \int_{D_p} e^\varphi dV \approx \frac{6}{\boldsymbol{\theta}_{k\ell} \cdot \mathbf{T}_{k\ell}^D} \left(\frac{e^{\varphi_i}}{(\boldsymbol{\theta}_{ij} \cdot \mathbf{T}_{ij}^D)(\boldsymbol{\theta}_{i\ell} \cdot \mathbf{T}_{i\ell}^D)} - \frac{e^{\varphi_j}}{(\boldsymbol{\theta}_{ij} \cdot \mathbf{T}_{ij}^D)(\boldsymbol{\theta}_{j\ell} \cdot \mathbf{T}_{j\ell}^D)} \right. \\ \left. + \frac{e^{\varphi_\ell}}{(\boldsymbol{\theta}_{j\ell} \cdot \mathbf{T}_{j\ell}^D)(\boldsymbol{\theta}_{i\ell} \cdot \mathbf{T}_{i\ell}^D)} \right) - \frac{6}{\boldsymbol{\theta}_{k\ell} \cdot \mathbf{T}_{k\ell}^D} \left(\frac{e^{\varphi_i}}{(\boldsymbol{\theta}_{ij} \cdot \mathbf{T}_{ij}^D)(\boldsymbol{\theta}_{ik} \cdot \mathbf{T}_{ik}^D)} \right. \\ \left. - \frac{e^{\varphi_j}}{(\boldsymbol{\theta}_{ij} \cdot \mathbf{T}_{ij}^D)(\boldsymbol{\theta}_{jk} \cdot \mathbf{T}_{jk}^D)} + \frac{e^{\varphi_k}}{(\boldsymbol{\theta}_{jk} \cdot \mathbf{T}_{jk}^D)(\boldsymbol{\theta}_{ik} \cdot \mathbf{T}_{ik}^D)} \right),$$

which is exact if $\boldsymbol{\theta}$ is a constant on the element.

Remark 3.3. Recall that the goal of this scheme is to yield a stable method for the convection-diffusion equation in the convection-dominated case. In other words, the mimetic scheme should handle the case when the diffusion coefficient tends to zero, $\alpha \rightarrow 0$. As φ scales with α^{-1} , this means that $\varphi \rightarrow \pm\infty$. Thus, for proper implementation of \mathcal{J}_D^0 , \mathcal{J}_D^1 , and \mathcal{J}_V^2 , we must consider numerical stability with floating point arithmetic to avoid overflow. For example, substituting (3.22) into the denominator of (3.9) yields

$$(\mathcal{J}_D^0 u)_{ij}^D = \left[\left(\frac{\boldsymbol{\theta}_{ij} \cdot \mathbf{T}_{ij}^D}{1 - e^{\varphi_i - \varphi_j}} \right) u_j^D - \left(\frac{\boldsymbol{\theta}_{ij} \cdot \mathbf{T}_{ij}^D}{e^{\varphi_j - \varphi_i} - 1} \right) u_i^D \right] \frac{\zeta(i, j)}{|\mathbf{e}_{ij}^D|}.$$

The problematic case is when $\varphi_i \rightarrow \varphi_j$, which makes the denominator of both terms zero. Taking the Taylor expansion of φ at $\boldsymbol{\theta}_{ij}$, or the constant approximation of $\boldsymbol{\theta} = \text{grad } \varphi$ on the edge \mathbf{e}_{ij}^D , gives $\boldsymbol{\theta}_{ij} \cdot \mathbf{T}_{ij}^D \approx \varphi_j - \varphi_i$. Therefore,

$$\lim_{\varphi_i \rightarrow \varphi_j} \frac{\boldsymbol{\theta}_{ij} \cdot \mathbf{T}_{ij}^D}{1 - e^{\varphi_i - \varphi_j}} \approx \lim_{\varphi_i \rightarrow \varphi_j} \frac{\varphi_j - \varphi_i}{1 - e^{\varphi_i - \varphi_j}} = 1, \\ \lim_{\varphi_i \rightarrow \varphi_j} \frac{\boldsymbol{\theta}_{ij} \cdot \mathbf{T}_{ij}^D}{e^{\varphi_j - \varphi_i} - 1} \approx \lim_{\varphi_i \rightarrow \varphi_j} \frac{\varphi_j - \varphi_i}{e^{\varphi_j - \varphi_i} - 1} = 1.$$

These limits imply that when $\varphi_i \rightarrow \varphi_j$,

$$(\mathcal{J}_D^0 u)_{ij}^D \approx \frac{u_j^D - u_i^D}{|\mathbf{e}_{ij}^D|} \zeta(i, j),$$

which is the standard MFD gradient (2.4). In the numerical results below, we identify when $|\varphi_i - \varphi_j| \leq 10^{-12}$ and replace the corresponding entries of \mathcal{J}_D^0 with the usual MFD gradient scheme. Similar approaches are performed for \mathcal{J}_D^1 and \mathcal{J}_V^2 , and details can be found in [29].

4. Analysis of the MFD method. By drawing connections between the proposed MFD scheme and SAFE, we provide a path to a concise and straightforward analysis of the MFD in the FE framework. In this section, we examine the connections to prove well-posedness and derive error estimates for MFD. We also show the stability, i.e., the monotonicity, of the MFD discretization (3.16) for the scalar convection-diffusion equation (1.1).

4.1. Equivalence between MFD and SAFE. Defining $\mathcal{E}_\varphi u := e^\varphi u$, the weak formulations of the convection-diffusion equations are: for $k = 0, 1, 2$, find $u \in H_0(\mathfrak{D}^k)$, such that

$$(4.1) \quad a(u, v) := \langle \alpha J^k u, \mathfrak{D}^k v \rangle + \langle \gamma u, v \rangle = \langle \alpha \mathcal{E}_{-\varphi} \mathfrak{D}^k \mathcal{E}_\varphi u, \mathfrak{D}^k v \rangle + \langle \gamma u, v \rangle = \langle f, v \rangle,$$

for all $v \in H_0(\mathfrak{D}^k)$. Note that $H_0(\mathfrak{D}^k)$ indicates the Sobolev space $H(\mathfrak{D}^k)$ with appropriate homogeneous Dirichlet boundary conditions applied. Then, the FE formulation is: for $k = 0, 1, 2$, find $u_h \in H_{h,0}(\mathfrak{D}^k)$, such that

$$(4.2) \quad a(u_h, v_h) = \langle \alpha J^k u_h, \mathfrak{D}^k v_h \rangle + \langle \gamma u_h, v_h \rangle = \langle \alpha \mathcal{E}_{-\varphi} \mathfrak{D}^k \mathcal{E}_\varphi u_h, \mathfrak{D}^k v_h \rangle + \langle \gamma u_h, v_h \rangle = \langle f, v_h \rangle,$$

for all $v_h \in H_{h,0}(\mathfrak{D}^k)$. The SAFE scheme uses properties of the canonical interpolation, Π^k in (2.3), to show that

$$\Pi^k \mathcal{E}_\varphi w_h = \sum_{s_i^k \in \mathcal{T}} \left(\int_{s_i^k} e^\varphi d\mathbf{x} \right) \eta_i^k(w_h) \lambda_i^k, \quad \forall w_h \in H_h(\mathfrak{D}^k),$$

and then defines the so-called *simplex-averaged* operator $\mathcal{H}_\varphi^k : H_h(\mathfrak{D}^k) \mapsto H_h(\mathfrak{D}^k)$,

$$\mathcal{H}_\varphi^k w_h = \sum_{s_i^k \in \mathcal{T}} \left(\int_{s_i^k} e^\varphi d\mathbf{x} \right)^{-1} \eta_i^k(w_h) \lambda_i^k, \quad \forall w_h \in H_h(\mathfrak{D}^k).$$

With these definitions, $\mathcal{H}_\varphi^k = (\Pi^k \mathcal{E}_\varphi)^{-1}$ on $H_h(\mathfrak{D}^k)$, implying that $\mathcal{H}_\varphi^k \Pi^k \mathcal{E}_\varphi = I$ on $H_h(\mathfrak{D}^k)$ (or $\mathcal{H}_\varphi^k \Pi^k \mathcal{E}_\varphi \approx I$, more generally). Then, the SAFE scheme yields the following approximation:

$$\mathcal{E}_{-\varphi} \mathfrak{D}^k \mathcal{E}_\varphi \approx (\mathcal{H}_\varphi^{k+1} \Pi^{k+1} \mathcal{E}_\varphi) (\mathcal{E}_{-\varphi} \mathfrak{D}^k \mathcal{E}_\varphi) = \mathcal{H}_\varphi^{k+1} \Pi^{k+1} \mathfrak{D}^k \mathcal{E}_\varphi = \mathcal{H}_\varphi^{k+1} \mathfrak{D}^k \Pi^k \mathcal{E}_\varphi,$$

where we use the commutative property, $\Pi^{k+1} \mathfrak{D}^k = \mathfrak{D}^k \Pi^k$, in the last step. Then, the SAFE scheme is: for $k = 0, 1, 2$, find $u_h \in H_{h,0}(\mathfrak{D}^k)$, such that

$$(4.3) \quad a_{\text{SAFE}}(u_h, v_h) = \langle \alpha \mathcal{H}_\varphi^{k+1} \mathfrak{D}^k \Pi^k \mathcal{E}_\varphi u_h, \mathfrak{D}^k v_h \rangle + \langle \gamma u_h, v_h \rangle = \langle f, v_h \rangle,$$

for all $v_h \in H_{h,0}(\mathfrak{D}^k)$.

Remark 4.1. As outlined in [63], (4.3) requires the assembly of a weighted mass matrix in $H_h(\mathfrak{D}^{k+1})$. Based on the idea proposed in [65], a local constant interpolation is constructed to modify the bilinear form to avoid the explicit construction of the weighted mass matrix. However, the presented MFD scheme more closely resembles (4.3) via mass-lumping and left scaling as discussed later in this subsection, so we only consider (4.3) here.

As in [1, 53], we use the method of mass lumping [10, 11, 16, 59] to draw connections to the MFD scheme. This allows us to acquire a diagonal approximation of the two weighted mass matrices arising from the two weighted L^2 inner products on $H_h(\mathfrak{D}^k)$ and $H_h(\mathfrak{D}^{k+1})$ in (4.3). To handle the weights α and γ , we use the canonical interpolation Π^k first and then apply the usual mass-lumping technique. This leads to the weak formulation of the MFD scheme: for $k = 0, 1, 2$, find $u_h \in H_{h,0}(\mathfrak{D}^k)$, such that

$$(4.4) \quad a_{\text{MFD}}(u_h, v_h) = \langle \Pi^{k+1} (\alpha \mathcal{H}_\varphi^{k+1} \mathfrak{D}^k \Pi^k \mathcal{E}_\varphi u_h), \mathfrak{D}^k v_h \rangle_h + \langle \Pi^k (\gamma u_h), v_h \rangle_h = \langle \Pi^k f, v_h \rangle_h,$$

for all $v_h \in H_{h,0}(\mathfrak{D}^k)$. Here, $\langle \cdot, \cdot \rangle_h$ denotes the corresponding mass-lumping.

To make the equivalence clear, consider the scalar convection-diffusion equation first ($k = 0$) and ignore the boundary conditions for now. In this case, the matrix representation of a_{SAFE} is

$$a_{\text{SAFE}}(u_h, v_h) = v_D^T (G_{\text{FE}}^T \mathcal{M}_{\alpha,1} E_{e^D}^{-1} G_{\text{FE}} E_{x^D} + \mathcal{M}_{\gamma,0}) u_D$$

where u_D and v_D are vector representations of u_h and v_h , respectively, and $\mathcal{M}_{\alpha,1}$ and $\mathcal{M}_{\gamma,0}$ are weighted mass matrices in $\mathbf{H}_h(\mathfrak{D}^1) = \mathbf{H}_h(\text{curl})$ and $\mathbf{H}_h(\mathfrak{D}^0) = H_h(\text{grad})$, respectively.

Defining the mass-lumped mass matrix of $H_h(\mathfrak{D}^k)$ as $\widetilde{\mathcal{M}}_k$ for $k = 0, 1, 2$, we obtain

$$\mathcal{M}_{\gamma,0} \approx \widetilde{\mathcal{M}}_0 \mathcal{D}_{\gamma,x^D} = \mathcal{D}_V \mathcal{D}_{\gamma,x^D}, \quad \mathcal{M}_{\alpha,1} \approx \widetilde{\mathcal{M}}_1 \mathcal{D}_{\alpha,e^D} = \mathcal{D}_{e^D} \mathcal{D}_{\partial V} \mathcal{D}_{\alpha,e^D},$$

where, \mathcal{D}_{γ,x^D} and \mathcal{D}_{α,e^D} are defined in (3.20) and (3.19), respectively. Full derivations are found in [1, 29]. Thus,

$$\begin{aligned} a_{\text{MFD}}(u_h, v_h) &= v_D^T (G_{\text{FE}}^T \mathcal{D}_{e^D} \mathcal{D}_{\partial V} \mathcal{D}_{\alpha,e^D} E_{e^D}^{-1} G_{\text{FE}} E_{x^D} + \mathcal{D}_V \mathcal{D}_{\gamma,x^D}) u_D \\ &= v_D^T (G^T \mathcal{D}_{\partial V} \mathcal{D}_{\alpha,e^D} \mathcal{J}_D^0 + \mathcal{D}_V \mathcal{D}_{\gamma,x^D}) u_D. \end{aligned}$$

Left scaling by \mathcal{D}_V^{-1} and using the fact $\text{div}_D = \mathcal{D}_V^{-1} G^T \mathcal{D}_{\partial V}$, the left-hand side of the MFD system (3.16) is *exactly* recovered. Noting that $\langle \Pi^0 f, v_h \rangle_h = v_D^T \widetilde{\mathcal{M}}_0 f_D$ with f_D defined in (3.21), the same left scaling recovers the right-hand side as well.

Similar arguments extend to the vector convection-diffusion equations (case $k = 1$ and $k = 2$). The mass-lumped weighted mass matrices are defined as

$$\begin{aligned} \mathcal{M}_{\gamma,1} &\approx \widetilde{\mathcal{M}}_1 \mathcal{D}_{\gamma,e^D} = \mathcal{D}_{e^D} \mathcal{D}_{\partial V} \mathcal{D}_{\gamma,e^D}, & \mathcal{M}_{\alpha,2} &\approx \widetilde{\mathcal{M}}_2 \mathcal{D}_{\alpha,e^V} = \mathcal{D}_{\partial D} \mathcal{D}_{e^V} \mathcal{D}_{\alpha,e^V}, \\ \mathcal{M}_{\gamma,2} &\approx \widetilde{\mathcal{M}}_2 \mathcal{D}_{\gamma,e^V} = \mathcal{D}_{\partial D} \mathcal{D}_{e^V} \mathcal{D}_{\gamma,e^V}, & \mathcal{M}_{\alpha,3} &\approx \widetilde{\mathcal{M}}_3 \mathcal{D}_{\alpha,x^V} = \mathcal{D}_D \mathcal{D}_{\alpha,x^V}, \end{aligned}$$

and lead to the weak formulation of the MFD scheme, (4.4). Then, for $k = 1$, applying the left scaling $\mathcal{D}_{\partial V}^{-1} \mathcal{D}_{e^D}^{-1}$, the MFD matrix system (3.17) is recovered. For $k = 2$, left scaling by $\mathcal{D}_{e^V}^{-1} \mathcal{D}_{\partial D}^{-1}$ leads to the MFD matrix system (3.18).

Remark 4.2. Based on the equivalence between the SAFE and MFD scheme, we see that the MFD scheme (4.4) provides another way to avoid assembly of the weighted mass matrix in $H_h(\mathfrak{D}^{k+1})$, since the mass-lumping only uses the geometric information of the meshes.

Remark 4.3. Although our discussion ignores the Dirichlet boundary conditions, the connection still holds after applying them properly on both the SAFE and MFD stiffness matrices.

4.2. Well-posedness and Error Analysis. Next, the well-posedness and error analysis of the MFD scheme for the convection-diffusion problems are considered. Note that the only difference between the weak formulation of the MFD method (4.4) and the MFD systems (3.16)–(3.18) is the left scaling, which does not affect the numerical solutions.

We first give some useful lemmas that are crucial to our theoretical analysis. First, we define an interpolation $\widetilde{\Pi}_\varphi^k : H(\mathfrak{D}^k) \mapsto H_h(\mathfrak{D}^k)$ defined as $\widetilde{\Pi}_\varphi^k v := \mathcal{H}_\varphi^k \Pi^k \mathcal{E}_\varphi v$. In [63], it has been shown that $\widetilde{\Pi}_\varphi^k v_h = v_h$ for any $v_h \in H_h(\mathfrak{D}^k)$, and, in general, has the following property:

LEMMA 4.4 ([63]). For $T \in \mathcal{T}$, if $v \in W^{1,p}(T)$ and $p > d$, where d is the dimension, then,

$$\|v - \tilde{\Pi}_\varphi^k v\| \leq Ch^{1+d(\frac{1}{2}-\frac{1}{p})} \left(\sum_{T \in \mathcal{T}} |v|_{1,p,T}^2 \right)^{\frac{1}{2}}.$$

For $v \in L^\infty(T)$, $T \in \mathcal{T}$,

$$\|\tilde{\Pi}_\varphi^k v\| \leq Ch^{\frac{d}{2}} \left(\sum_{T \in \mathcal{T}} \|v\|_{0,\infty,T}^2 \right)^{\frac{1}{2}}.$$

where the constant C depends on p and the Sobolev embedding number.

Proof. The proof can be found in Lemma 5.1 and Corollary 5.2 of [63]. \square

Since the connection between the SAFE and MFD methods depends on the mass-lumping, we assume the following mass-lumping error estimates holds [16, 59]:

$$(4.5) \quad |\langle w_h, v_h \rangle - \langle w_h, v_h \rangle_h| \leq Ch^2 \|w_h\|_{H(\mathfrak{D}^k)} \|v_h\|_{H(\mathfrak{D}^k)}, \quad \forall w_h, v_h \in H_h(\mathfrak{D}^k),$$

where $C > 0$ is a constant depending on the shape regularity of the mesh. Based on the mass-lumping error (4.5), we have the following lemma which bounds the difference between the SAFE and MFD methods.

LEMMA 4.5. For any positive weight function, $0 < \mu(\mathbf{x}) \in W^{1,\infty}(\Omega)$, assuming the mass-lumping error estimate, (4.5), holds, then, we have for any $w_h, v_h \in H_h(\mathfrak{D}^k)$,

$$|\langle \mu w_h, v_h \rangle - \langle \Pi^k(\mu w_h), v_h \rangle_h| \leq Ch \|\mu\|_{1,\infty} \|w_h\| \|v_h\|_{H(\mathfrak{D}^k)},$$

where the constant $C > 0$ does not depend on μ .

Proof. For any $w_h, v_h \in H_h(\mathfrak{D}^k)$,

$$(4.6) \quad \begin{aligned} \langle \mu w_h, v_h \rangle - \langle \Pi^k(\mu w_h), v_h \rangle_h &= \langle \mu w_h - \Pi^k(\mu w_h), v_h \rangle \\ &\quad + (\langle \Pi^k(\mu w_h), v_h \rangle - \langle \Pi^k(\mu w_h), v_h \rangle_h). \end{aligned}$$

Note that $w_h = \sum_{s_i^k} \eta_i^k(w_h) \lambda_i^k$ and $\Pi^k(\mu w_h) = \sum_{s_i^k} \left(\int_{s_i^k} \mu \, d\mathbf{x} \right) \eta_i^k(w_h) \lambda_i^k$. Then,

$$\begin{aligned} &|\langle \mu w_h - \Pi^k(\mu w_h), v_h \rangle| \\ &\leq \|\mu w_h - \Pi^k(\mu w_h)\| \|v_h\| = \left\| \sum_{s_i^k} \left(\mu - \int_{s_i^k} \mu \, d\mathbf{x} \right) \eta_i^k(w_h) \lambda_i^k \right\| \|v_h\| \\ &\leq \|\mu - \int_{s_i^k} \mu \, d\mathbf{x}\|_{0,\infty} \|w_h\| \|v_h\| \leq Ch \|\mu\|_{1,\infty} \|w_h\| \|v_h\| \end{aligned}$$

For the second term on the right-hand side of (4.6), apply the mass-lumping error estimates (4.5), an inverse inequality, and the stability of Π^k , to get

$$\begin{aligned} |\langle \Pi^k(\mu w_h), v_h \rangle - \langle \Pi^k(\mu w_h), v_h \rangle_h| &\leq Ch^2 \|\Pi^k(\mu w_h)\|_{H(\mathfrak{D}^k)} \|v_h\|_{H(\mathfrak{D}^k)} \\ &\leq Ch \|\Pi^k(\mu w_h)\| \|v_h\|_{H(\mathfrak{D}^k)} \\ &\leq Ch \|\mu\|_{0,\infty} \|w_h\| \|v_h\|_{H(\mathfrak{D}^k)} \end{aligned}$$

Combining the two results completes the proof. \square

Now we are ready to present an important lemma which measures the consistency between the bilinear forms $a(\cdot, \cdot)$ from (4.2) and $a_{\text{MFD}}(\cdot, \cdot)$ from (4.4), using the intermediary $a_{\text{SAFE}}(\cdot, \cdot)$ from (4.3).

LEMMA 4.6. *Assume $\alpha, \gamma \in W^{1,\infty}(\Omega)$, $\theta \in W^{0,\infty}(\Omega)$ and the assumptions for the mass-lumping error estimate, (4.5), are satisfied. Then, for any $w_h, v_h \in H_h(\mathfrak{D}^k)$, the following estimate holds,*

$$|a(w_h, v_h) - a_{\text{MFD}}(w_h, v_h)| \leq c_p h \|w_h\|_{H(\mathfrak{D}^k)} \|v_h\|_{H(\mathfrak{D}^k)},$$

where $c_p := C_1 \|\alpha\|_{0,\infty} \|\theta\|_{0,\infty} + C_3 \|\alpha\|_{1,\infty} (1 + \|\theta\|_{0,\infty}) + C_2 \|\gamma\|_{1,\infty} > 0$ with C_1, C_2 , and C_3 being generic positive constants that do not depend on α, θ , and γ .

Proof. For any $w_h, v_h \in H(\mathfrak{D}^k)$, we have

$$a(w_h, v_h) - a_{\text{MFD}}(w_h, v_h) = a(w_h, v_h) - a_{\text{SAFE}}(w_h, v_h) + a_{\text{SAFE}}(w_h, v_h) - a_{\text{MFD}}(w_h, v_h).$$

Since $H_\varphi^{k+1} \mathfrak{D}^k \Pi^k \mathcal{E}_\varphi = \tilde{\Pi}_\varphi^{k+1} J^k$,

$$\begin{aligned} |a(w_h, v_h) - a_{\text{SAFE}}(w_h, v_h)| &= \left| \langle \alpha (I - \tilde{\Pi}_\varphi^{k+1}) J^k w_h, \mathfrak{D}^k v_h \rangle \right| \\ &\leq \|\alpha\|_{0,\infty} \|(I - \tilde{\Pi}_\varphi^{k+1}) J^k w_h\| \|\mathfrak{D}^k v_h\| \\ &\leq C_1 \|\alpha\|_{0,\infty} h^{1+d(\frac{1}{2}-\frac{1}{p})} \left(\sum_{T \in \mathcal{T}} |J^k w_h|_{1,p,T}^2 \right)^{\frac{1}{2}} \|\mathfrak{D}^k v_h\| \\ &\leq C_1 \|\alpha\|_{0,\infty} \|\theta\|_{0,\infty} h \|w_h\|_{H(\mathfrak{D}^k)} \|\mathfrak{D}^k v_h\| \end{aligned}$$

Here, we use $|\mathfrak{D}^k w_h|_{1,p,T} = 0$ for any $w_h \in H_h(\mathfrak{D}^k)$ and an inverse inequality in the last step. Next we estimate the difference between a_{SAFE} and a_{MFD} ,

$$\begin{aligned} &|a_{\text{SAFE}}(w_h, v_h) - a_{\text{MFD}}(w_h, v_h)| \\ &\leq \left| \langle \alpha \tilde{\Pi}_\varphi^{k+1} J^k w_h, \mathfrak{D}^k v_h \rangle - \langle \Pi^{k+1}(\alpha \tilde{\Pi}_\varphi^{k+1} J^k w_h), \mathfrak{D}^k v_h \rangle_h \right| \\ &\quad + \left| \langle \gamma w_h, v_h \rangle - \langle \Pi^k(\gamma w_h), v_h \rangle_h \right| \end{aligned}$$

By Lemma 4.5, we have $|\langle \gamma w_h, v_h \rangle - \langle \Pi^k(\gamma w_h), v_h \rangle_h| \leq C_2 \|\gamma\|_{1,\infty} h \|w_h\| \|v_h\|_{H(\mathfrak{D}^k)}$. Similarly, using Lemma 4.5,

$$\begin{aligned} &\left| \langle \alpha \tilde{\Pi}_\varphi^{k+1} J^k w_h, \mathfrak{D}^k v_h \rangle - \langle \Pi^{k+1}(\alpha \tilde{\Pi}_\varphi^{k+1} J^k w_h), \mathfrak{D}^k v_h \rangle_h \right| \\ &\leq C \|\alpha\|_{1,\infty} h \|\tilde{\Pi}_\varphi^{k+1} J^k w_h\| \|v_h\|_{H(\mathfrak{D}^k)} \end{aligned}$$

Based on Lemma 4.4 and an inverse inequality,

$$\begin{aligned} \|\tilde{\Pi}_\varphi^{k+1} J^k w_h\|^2 &\leq C h^d \sum_{T \in \mathcal{T}} \|J^k w_h\|_{0,\infty,T}^2 \\ &\leq C \sum_{T \in \mathcal{T}} \left(h^{\frac{d}{2}} \|\mathfrak{D}^k w_h\|_{0,\infty,T} + \|\theta\|_{0,\infty,T} h^{\frac{d}{2}} \|w_h\|_{0,\infty,T} \right)^2 \\ &\leq C(1 + \|\theta\|_{0,\infty}) \|w_h\|_{H(\mathfrak{D}^k)}. \end{aligned}$$

Therefore,

$$\begin{aligned} & \left| \langle \alpha \tilde{\Pi}_\varphi^{k+1} J^k w_h, \mathfrak{D}^k v_h \rangle - \langle \Pi^{k+1}(\alpha \tilde{\Pi}_\varphi^{k+1} J^k w_h), \mathfrak{D}^k v_h \rangle_h \right| \\ & \leq C_3 \|\alpha\|_{1,\infty} (1 + \|\boldsymbol{\theta}\|_{0,\infty}) h \|w_h\|_{H(\mathfrak{D}^k)} \|v_h\|_{H(\mathfrak{D}^k)}. \end{aligned}$$

This implies that

$$|a_{\text{SAFE}}(w_h, v_h) - a_{\text{MFD}}(w_h, v_h)| \leq \tilde{C} h \|w_h\|_{H(\mathfrak{D}^k)} \|v_h\|_{H(\mathfrak{D}^k)},$$

where the constant $\tilde{C} := C_3 \|\alpha\|_{1,\infty} (1 + \|\boldsymbol{\theta}\|_{0,\infty}) + C_2 \|\gamma\|_{1,\infty} > 0$. Overall,

$$|a(w_h, v_h) - a_{\text{MFD}}(w_h, v_h)| \leq c_p h \|w_h\|_{H(\mathfrak{D}^k)} \|v_h\|_{H(\mathfrak{D}^k)},$$

which completes the proof with $c_p := C_1 \|\alpha\|_{0,\infty} \|\boldsymbol{\theta}\|_{0,\infty} + C_3 \|\alpha\|_{1,\infty} (1 + \|\boldsymbol{\theta}\|_{0,\infty}) + C_2 \|\gamma\|_{1,\infty} > 0$. \square

4.2.1. Well-posedness. We assume the continuous problem (4.1) is well-posed, i.e.,

$$(4.7) \quad \sup_{w \in H_0(\mathfrak{D}^k)} \sup_{v \in H_0(\mathfrak{D}^k)} \frac{|a(w, v)|}{\|w\|_{H(\mathfrak{D}^k)} \|v\|_{H(\mathfrak{D}^k)}} = c_b > 0,$$

and

$$(4.8) \quad \inf_{w \in H_0(\mathfrak{D}^k)} \sup_{v \in H_0(\mathfrak{D}^k)} \frac{|a(w, v)|}{\|w\|_{H(\mathfrak{D}^k)} \|v\|_{H(\mathfrak{D}^k)}} = c_i > 0,$$

where the constants c_b and c_i may depend on α , $\boldsymbol{\beta}$, and γ .

The main tool to show the well-posedness of the weak-formulation of the MFD scheme, (4.4), is [Lemma 4.6](#). First, we show that the MFD bilinear form, a_{MFD} , is bounded, and then that it satisfies an inf-sup condition.

LEMMA 4.7 (Boundedness of a_{MFD}). *Under the same assumptions of [Lemma 4.6](#) and assuming (4.7),*

$$(4.9) \quad \sup_{w_h \in H_{h,0}(\mathfrak{D}^k)} \sup_{v_h \in H_{h,0}(\mathfrak{D}^k)} \frac{|a_{\text{MFD}}(w_h, v_h)|}{\|w_h\|_{H(\mathfrak{D}^k)} \|v_h\|_{H(\mathfrak{D}^k)}} = \tilde{c}_b > 0,$$

Proof. Using (4.7) and [Lemma 4.6](#),

$$\begin{aligned} |a_{\text{MFD}}(w_h, v_h)| & \leq |a(w_h, v_h)| + |a_{\text{MFD}}(w_h, v_h) - a(w_h, v_h)| \\ & \leq c_b \|w_h\|_{H(\mathfrak{D}^k)} \|v_h\|_{H(\mathfrak{D}^k)} + c_p h \|w_h\|_{H(\mathfrak{D}^k)} \|v_h\|_{H(\mathfrak{D}^k)} \\ & = \tilde{c}_b \|w_h\|_{H(\mathfrak{D}^k)} \|v_h\|_{H(\mathfrak{D}^k)}, \end{aligned}$$

which implies (4.9) with $\tilde{c}_b = c_b + c_p h$. \square

LEMMA 4.8 (Inf-sup condition of a_{MFD}). *Under the same assumptions of [Lemma 4.6](#) and assuming (4.8), for sufficiently small h ,*

$$(4.10) \quad \inf_{w_h \in H_{h,0}(\mathfrak{D}^k)} \sup_{v_h \in H_{h,0}(\mathfrak{D}^k)} \frac{|a_{\text{MFD}}(w_h, v_h)|}{\|w_h\|_{H(\mathfrak{D}^k)} \|v_h\|_{H(\mathfrak{D}^k)}} = \tilde{c}_i > 0.$$

Proof. According to the continuous inf-sup condition, (4.8), for any given $v_h \in H_{h,0}(\mathfrak{D}^k)$, there exists $w_h \in H_{h,0}(\mathfrak{D}^k)$ such that $\frac{|a(w_h, v_h)|}{\|v_h\|_{H(\mathfrak{D}^k)}} \geq c_i \|w_h\|_{H(\mathfrak{D}^k)}$. Using Lemma 4.6,

$$\begin{aligned} \frac{|a_{\text{MFD}}(w_h, v_h)|}{\|v_h\|_{H(\mathfrak{D}^k)}} &\geq \frac{|a(w_h, v_h)|}{\|v_h\|_{H(\mathfrak{D}^k)}} - \frac{|a_{\text{MFD}}(w_h, v_h) - a(w_h, v_h)|}{\|v_h\|_{H(\mathfrak{D}^k)}} \\ &\geq c_i \|w_h\|_{H(\mathfrak{D}^k)} - c_p h \|w_h\|_{H(\mathfrak{D}^k)} = \tilde{c}_i \|w_h\|_{H(\mathfrak{D}^k)}, \end{aligned}$$

where $\tilde{c}_i = c_i - c_p h > 0$ for sufficiently small h . This completes the proof. \square

Thus, we have the well-posedness of the MFD weak formulation (4.4) as follows.

THEOREM 4.9 (Well-posedness of the MFD weak formulation (4.4)). *Under the same assumptions of Lemma 4.6 and assuming that the bilinear form $a(\cdot, \cdot)$ from (4.2) satisfies the boundedness condition (4.7) and the inf-sup condition (4.8), for sufficiently small h , the MFD weak formulation, (4.4), is well-posed, i.e., it has a unique solution.*

Proof. The result follows from Lemma 4.7, Lemma 4.8, and Babuška's theory [6]. \square

4.2.2. Error Analysis. With the above well-posedness result, the error analysis of the MFD scheme, (4.4), follows from Strang's first lemma [58].

THEOREM 4.10. *Let u and u_h be the solutions of (4.1) and (4.4), respectively, and $f \in H(\mathfrak{D}^k)$. Under the same assumptions of Lemma 4.6 and assuming that the bilinear form $a(\cdot, \cdot)$ satisfies the boundedness condition, (4.7), and the inf-sup condition, (4.8), for sufficiently small h ,*

$$(4.11) \quad \|u - u_h\|_{H(\mathfrak{D}^k)} \leq \inf_{w_h \in H_{h,0}(\mathfrak{D}^k)} \left[\left(1 + \frac{c_b}{\tilde{c}_i} \right) \|u - w_h\|_{H(\mathfrak{D}^k)} + \frac{c_p}{\tilde{c}_i} h \|w_h\|_{H(\mathfrak{D}^k)} \right] + Ch \|f\|_{H(\mathfrak{D}^k)},$$

where constant c_b is the continuous upper bound from the assumption (4.7), \tilde{c}_i is the constant from the discrete inf-sup condition (4.10), c_p is the constant defined in Lemma 4.6, and the last constant C is a generic constant that does not depend on α , θ , and γ .

Proof. For any $w_h \in H_{h,0}(\mathfrak{D}^k)$, we have

$$\begin{aligned} a_{\text{MFD}}(u_h - w_h, v_h) &= a(u - w_h, v_h) + [a(w_h, v_h) - a_{\text{MFD}}(w_h, v_h)] + [\langle \Pi^k f, v_h \rangle_h - \langle f, v_h \rangle] \\ &\leq c_b \|u - w_h\|_{H(\mathfrak{D}^k)} \|v_h\|_{H(\mathfrak{D}^k)} + c_p h \|w_h\|_{H(\mathfrak{D}^k)} \|v_h\|_{H(\mathfrak{D}^k)} + Ch \|f\|_{H(\mathfrak{D}^k)} \|v_h\|_{H(\mathfrak{D}^k)}. \end{aligned}$$

By the discrete inf-sup condition (4.10), we arrive at

$$\begin{aligned} \|u_h - w_h\|_{H(\mathfrak{D}^k)} &\leq \tilde{c}_i^{-1} \sup_{v_h \in H_{h,0}(\mathfrak{D}^k)} \frac{|a_{\text{MFD}}(u_h - w_h, v_h)|}{\|v_h\|_{H(\mathfrak{D}^k)}} \\ &\leq \frac{c_b}{\tilde{c}_i} \|u - w_h\|_{H(\mathfrak{D}^k)} + \frac{c_p}{\tilde{c}_i} h \|w_h\|_{H(\mathfrak{D}^k)} + Ch \|f\|_{H(\mathfrak{D}^k)}. \end{aligned}$$

Then the error estimates (4.11) follows from the above inequality and the triangle inequality $\|u - u_h\|_{H(\mathfrak{D}^k)} \leq \|u - w_h\|_{H(\mathfrak{D}^k)} + \|u_h - w_h\|_{H(\mathfrak{D}^k)}$. \square

By choosing $w_h = \Pi^k u$ in Theorem 4.10, we have the following error estimates.

COROLLARY 4.11. *Let u and u_h be the solutions of (4.1) and (4.4), respectively. Furthermore, let $u \in H^2(\Omega)$ and $f \in H(\mathfrak{D}^k)$. Under the same assumptions of Theorem 4.10,*

$$\|u - u_h\|_{H(\mathfrak{D}^k)} \leq Ch (\|u\|_2 + \|f\|_{H(\mathfrak{D}^k)})$$

where C is a positive constant depending on α , θ , and γ .

Remark 4.12. If we assume h is small enough so that $\tilde{c}_i \leq c_i/2$, then the constant C in Corollary 4.11 is proportional to $\max\{\frac{c_b}{c_i}, \frac{c_p}{c_i}\}$, which implies that the above error estimate depends on $\|\theta\|_{0,\infty} = \|\frac{\beta}{\alpha}\|_{0,\infty}$. As expected for convection-dominated problems, this implies that when the ratio $|\alpha|/|\beta|$ gets smaller, the error gets bigger, and a sufficiently small h is needed to observe a proper convergence rate. In Section 5, our numerical experiments confirm this result.

Remark 4.13. The assumption that $f \in H(\mathfrak{D}^k)$ makes the error estimate sub-optimal in terms of the regularity requirement. This is due to the right-hand side, $\langle \Pi^k f, v_h \rangle_h$, used in the MFD scheme. If $\langle f, v_h \rangle$ is used, the assumption on $f \in H(\mathfrak{D}^k)$ is no longer needed, but does require that the right-hand sides of (3.16)–(3.18) be implemented accordingly.

4.3. Monotonicity for $H(\text{grad})$. Finally, we consider the monotonicity and stability of the scalar convection-diffusion problem, (1.1). Defining $\mathcal{L}u := -\text{div}(\alpha J^0 u) + \gamma u$, we note that \mathcal{L} satisfies a *maximum principle* or *monotonicity property*, which says the inverse of \mathcal{L} is nonnegative. More precisely, if $(\mathcal{L}u)(\mathbf{x}) > 0$ for all $\mathbf{x} \in \Omega$, then $u(\mathbf{x}) \geq 0$ for all $\mathbf{x} \in \Omega$. This property holds regardless of the ratio $|\beta(\mathbf{x})|/|\alpha(\mathbf{x})|$ and, therefore, is important when convection is dominating diffusion, i.e., $|\alpha(\mathbf{x})| \ll |\beta(\mathbf{x})|$.

In practice, it is crucial to construct a numerical scheme that preserves the monotonicity property discretely. In particular, if \mathcal{L}_h and f_h are discretizations of \mathcal{L} and f , respectively, then \mathcal{L}_h has the monotonicity property, if $f_h \geq 0$, implies $\mathcal{L}_h^{-1} f_h \geq 0$. Here, the operand, \geq , is understood in a component-wise fashion. It is also well-known from a linear algebra point of view, that if \mathcal{L}_h is a non-singular M-matrix, then it is monotone (see e.g. [52]).

The MFD scheme for the scalar convection-diffusion problem, (3.16) yields

$$\mathcal{L}_h = \text{div}_D \mathcal{D}_{\alpha, e^D} \mathcal{J}_D^0 + \mathcal{D}_{\gamma, \mathbf{x}^D} := \mathcal{D}_V^{-1} \mathcal{G}^T \mathcal{W} \mathcal{G} E_{\mathbf{x}^D} + \mathcal{D}_{\gamma, \mathbf{x}^D},$$

where \mathcal{W} is a diagonal matrix defined as $\mathcal{W} := \mathcal{D}_{\partial V} \mathcal{D}_{\alpha, e^D} E_{e^D}^{-1} \mathcal{D}_{e^D}$. Here, we assume the Dirichlet boundary conditions have been applied so that the rows and columns corresponding to the boundary nodes have been eliminated. The next theorem states that \mathcal{L}_h is a non-singular M-matrix, which implies the monotonicity of the MFD scheme, (3.16), for the scalar convection-diffusion problem (1.1).

THEOREM 4.14. *Let $\alpha(\mathbf{x}) > 0$ and $\gamma(\mathbf{x}) \geq 0$ for all $\mathbf{x} \in \Omega$. If a non-degenerate dual mesh configuration (e.g., non-degenerate Delaunay and Voronoi grids) is used, then the stiffness matrix \mathcal{L}_h of the MFD scheme, (3.16), is a non-singular M-matrix, i.e., it is monotone.*

Proof. Based on the non-degenerative assumption of the dual mesh configuration, the diagonal entries of the diagonal matrices, \mathcal{D}_V , $\mathcal{D}_{\partial V}$, \mathcal{D}_{e^D} , $E_{\mathbf{x}^D}$, and E_{e^D} are all positive. In addition, according to the assumptions on α and γ , the diagonal entries of $\mathcal{D}_{\alpha, e^D}$ are all positive and the diagonal entries of $\mathcal{D}_{\gamma, \mathbf{x}^D}$ are all non-negative. Therefore, the diagonal entries of the diagonal matrix \mathcal{W} are non-negative. Since \mathcal{G} is

the Delaunay edge-vertex signed incidence matrix (with the columns corresponding to the boundary nodes eliminated), the off-diagonal entries of \mathcal{L}_h are

$$(\mathcal{L}_h)_{ij} = (\mathcal{D}_V)_{ii}^{-1} (\mathcal{G}^T \mathcal{W} \mathcal{G})_{ij} (E_{\mathbf{x}^D})_{jj} = -(\mathcal{D}_V)_{ii}^{-1} (\mathcal{W})_{e_{ij}^D} (E_{\mathbf{x}^D})_{jj} \leq 0,$$

where $(\mathcal{W})_{e_{ij}^D}$ denotes the diagonal entry of \mathcal{W} corresponding to the edge e_{ij}^D , which incidents with nodes \mathbf{x}_i^D and \mathbf{x}_j^D . Therefore, \mathcal{L}_h is a Z-matrix (a matrix with all non-positive off-diagonal entries).

Defining the inner product $(u_D, v_D)_{E_{\mathbf{x}^D} \mathcal{D}_V} := v_D^T E_{\mathbf{x}^D} \mathcal{D}_V u_D$, we have

$$(\mathcal{L}_h u_D, v_D)_{E_{\mathbf{x}^D} \mathcal{D}_V} = v_D^T E_{\mathbf{x}^D} \mathcal{G}^T \mathcal{W} \mathcal{G} E_{\mathbf{x}^D} u_D + v_D^T E_{\mathbf{x}^D} \mathcal{D}_V \mathcal{D}_{\gamma, \mathbf{x}^D} u_D.$$

Therefore, \mathcal{L}_h is symmetric with respect to $(\cdot, \cdot)_{E_{\mathbf{x}^D} \mathcal{D}_V}$ and $(\mathcal{L}_h v_D, v_D)_{E_{\mathbf{x}^D} \mathcal{D}_V} \geq 0$ for any v_D . Furthermore, due to the well-posedness result [Theorem 4.9](#), we have $(\mathcal{L}_h v_D, v_D)_{E_{\mathbf{x}^D} \mathcal{D}_V} > 0$ for any $v_D \neq 0$. By the Courant minmax principle, all the eigenvalues of \mathcal{L}_h are real and positive. Since \mathcal{L}_h is also a Z-matrix, by one characterization given in [\[52\]](#), \mathcal{L}_h is a non-singular M-matrix. \square

Remark 4.15. The non-degenerate Delaunay and Voronoi grid configuration is one where every dual point lies in the interior of the primal element, guaranteeing positivity of mesh metrics. However, the assumption on the dual mesh configuration, specifically requiring a Delaunay primal mesh and Voronoi dual mesh, can be relaxed. Given a primal mesh, which implies \mathcal{D}_{e^D} has positive diagonal entries, as long as the dual mesh is reasonable in the sense that diagonal entries of $\mathcal{D}_{\partial V}$ and \mathcal{D}_V are all positive, the resulting MFD scheme is monotone.

Remark 4.16. [Theorem 4.14](#) assumes that the integrals used to define $\mathcal{D}_{\alpha, e^D}$ and E_{e^D} are computed exactly. In practice, numerical quadrature rules are used instead, but \mathcal{L}_h is still a non-singular M-matrix if the numerical quadrature rules preserve positivity. For computing $\mathcal{D}_{\alpha, e^D}$, standard numerical quadrature rules, such as the midpoint rule, preserve the positivity. For computing E_{e^D} , special attention is needed. However, it can be shown that the quadrature rule [\(3.22\)](#) introduced in [subsection 3.3.1](#) does preserve the positivity. Therefore, our implementation provides a monotone MFD discretization for the scalar convection-diffusion problem.

Remark 4.17. For the case of pure Neumann boundary condition, \mathcal{L}_h is singular and its kernel is spanned by constants. In this case, if we restrict ourselves to a subspace that is orthogonal to that kernel, then \mathcal{L}_h^{-1} is still well-defined and positive. Therefore, it is monotone.

Remark 4.18. The stability for the $\mathbf{H}(\text{curl})$ and $\mathbf{H}(\text{div})$ cases are more subtle than the $\mathbf{H}(\text{grad})$ case considered here. The stability cannot be simply explained or verified by the monotonicity of the corresponding stiffness matrices, and, in fact, the stiffness matrices are not monotone for both cases anymore. However, we still observe the stability of the MFD schemes numerically; see [Section 5](#) for details.

5. Numerical Results. To verify the theoretical results presented in this paper, the $\mathbf{H}(\text{grad})$ and $\mathbf{H}(\text{curl})$ schemes are implemented in two dimensions in MATLAB. Two types of meshes are designed to test the MFD method. The first uses a hexagonal domain (see [Figure 2](#)), which has a Delaunay triangulation for the primal mesh and a non-degenerate dual Voronoi mesh, meaning the Voronoi points lie within their corresponding Delaunay element. More resolved meshes are obtained through uniform refinement and the error estimates are verified on these grids. As many classical

convection-diffusion problems with jumps and boundary layers are simulated on the unit square, we design a primal Delaunay triangulation and dual Voronoi mesh on $[0, 1] \times [0, 1]$. The refinement method, which preserves non-degeneracy of the meshes, is demonstrated in Figure 3.

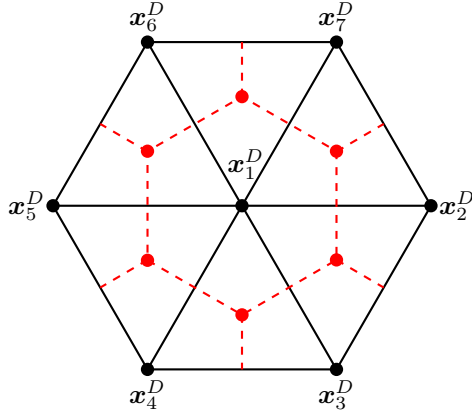


Fig. 2: Hexagonal computational domain with $h = 1$, centered at $(0, 0)$. The primal mesh is drawn with solid black lines and the dual mesh is shown in red dashed lines.

5.1. Convergence results. First, the error estimates given by Corollary 4.11 are verified. Here, the domain is the hexagonal domain as in Figure 2. For the $H(\text{grad})$ case, (1.1), the convergence is verified with the exact solution,

$$(5.1) \quad u(\mathbf{x}) = \sin(\pi x_1) \sin(\pi x_2),$$

where the right-hand side can be analytically computed. Similarly, the $\mathbf{H}(\text{curl})$ convergence results are verified using exact solution,

$$(5.2) \quad \mathbf{u}(\mathbf{x}) = \begin{bmatrix} \sin(\pi x_1) \sin(\pi x_2) \\ \cos(\pi x_1) \cos(\pi x_2) \end{bmatrix},$$

where the right-hand side can again be computed analytically via (1.2). In both cases, the convection coefficient is given by

$$\boldsymbol{\beta}(\mathbf{x}) = \begin{bmatrix} \cos(x_1) + 4 \\ -\sin(x_2) + 4 \end{bmatrix},$$

and we use $\gamma = 0$ and $\gamma = 1$ for the $H(\text{grad})$ and $\mathbf{H}(\text{curl})$ cases, respectively. To show the robustness of our schemes, particularly in the convection-dominated regime, we vary the diffusion coefficient α in our numerical experiments.

Figure 4 verifies the error estimates given by Theorem 4.10 and Corollary 4.11 for the $H(\text{grad})$ convection-diffusion problem. The top-left graph of Figure 4 reports the error in the $H(\text{grad})$ semi-norm, i.e., $|u - u_h|_1 := \|\text{grad}(u - u_h)\|$. We see that for $\alpha = 1, 10^{-1}$, and 10^{-2} the $\mathcal{O}(h)$ rate is eventually recovered as the mesh is refined. In general, we expect to see the trend that the rate approaches $\mathcal{O}(h)$ once $h < |\alpha|/|\boldsymbol{\beta}|$. For example, for $\alpha = 10^{-3}$ the convergence rate is heading toward $\mathcal{O}(h)$ as h gets

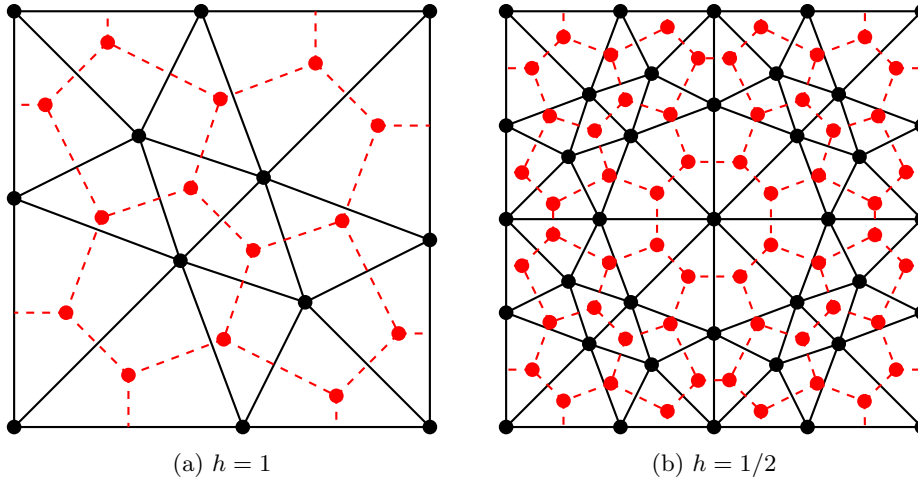


Fig. 3: Primal and dual mesh on the unit square, $[0, 1] \times [0, 1]$. The primal mesh is drawn with solid black lines and the dual mesh is shown in red dashed lines. A base, coarse mesh is shown in (a), and one refinement has been done in (b).

closer to 10^{-3} (since $\beta \sim \mathcal{O}(1)$). More refinement is needed to see a similar result for $\alpha = 10^{-4}$ and 10^{-5} . This is consistent with our theoretical results, which require h to be sufficiently small.

Since the MFD scheme can be considered as a mass-lumped SAFE scheme, in the L^2 norm, we would expect the error to converge as $\mathcal{O}(h^2)$ for sufficiently small h . This is numerically verified in the top-right graph of Figure 4. For small α , we see closer to $\mathcal{O}(h)$ convergence, which asymptotically approaches $\mathcal{O}(h^2)$ with finer meshes, whereas the large values of α clearly demonstrate the $\mathcal{O}(h^2)$ convergence. Once again, the turn from $\mathcal{O}(h)$ to $\mathcal{O}(h^2)$ happens roughly when h becomes smaller than $|\alpha|/|\beta|$.

Next, we examine the convergence of the $\mathbf{H}(\text{curl})$ convection-diffusion problem. The $\mathbf{H}(\text{curl})$ semi-norm error, i.e., $\|\mathbf{u} - \mathbf{u}_h\|_{\mathbf{H}(\text{curl})} := \|\text{curl}(\mathbf{u} - \mathbf{u}_h)\|$, is plotted in the bottom-left graph of Figure 4. When the mesh spacing, h , is larger than $|\alpha|/|\beta|$, poor convergence is observed. However, the expected $\mathcal{O}(h)$ convergence is observed when $h \leq |\alpha|/|\beta|$. In particular, we see the $\alpha = 10^{-3}$ case begin to trend toward $\mathcal{O}(h)$ around $h = 10^{-3}$. As in the $H(\text{grad})$ case, more refinement is needed to verify the convergence for smaller values of α . The bottom-right graph of Figure 4 also demonstrates $\mathcal{O}(h)$ convergence in the L^2 norm, which is expected due to the connection between our MFD scheme and the SAFE method (for the $\mathbf{H}(\text{curl})$ case, the SAFE discretization uses the lowest-order Nédélec elements).

5.2. Boundary and internal layer in $H(\text{grad})$. Next, we examine the stability of the $H(\text{grad})$ scheme on the domain $\Omega = [0, 1] \times [0, 1]$ using the meshes given by Figure 3, with $h = 1/64$. First, we consider a simple example which admits a jump at the boundary, using parameters,

$$(5.3) \quad \alpha = 10^{-6}, \quad \beta = \begin{bmatrix} 2 + x_1 \\ 1 + x_2 \end{bmatrix}, \quad \gamma = 0, \quad f = 1,$$

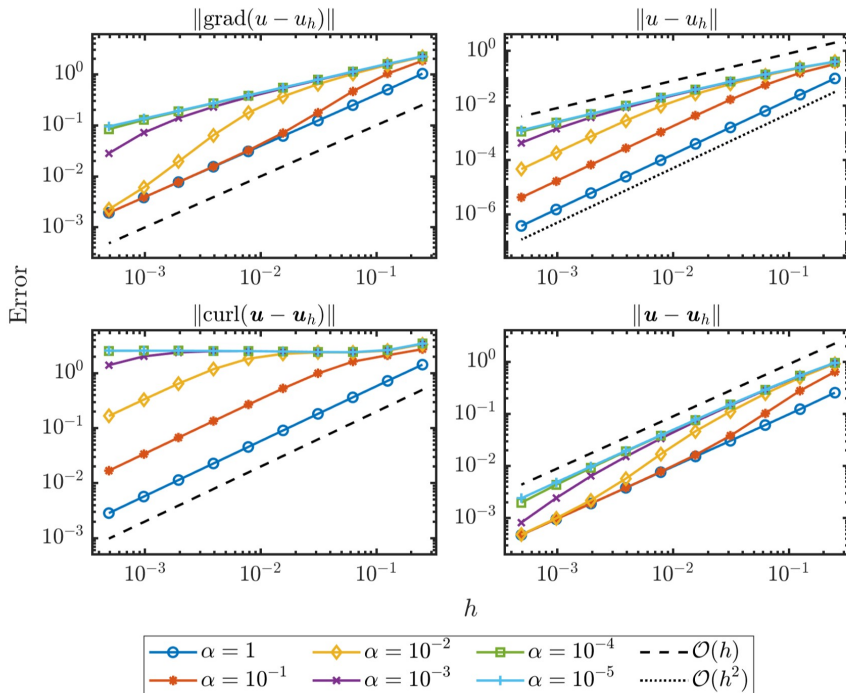
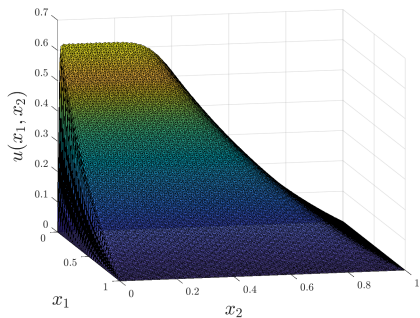
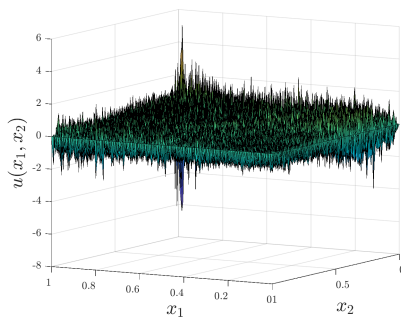


Fig. 4: MFD results for solving the convection-diffusion equations with various values of α on a hexagonal computational domain. (Top) Error versus h for scalar equation (3.16) with exact solution (5.1) with error measured in the (left) $H(\text{grad})$ semi-norm and (right) L^2 norm. (Bottom) Error versus h for vector equation (3.17) with exact solution (5.2) with error measured in (left) $\mathbf{H}(\text{curl})$ semi-norm and (right) L^2 norm.



(a) MFD solution of (3.16).



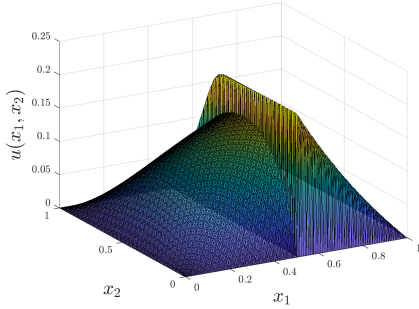
(b) Linear Lagrange FEM solution of (1.1).

Fig. 5: Comparison of MFD and FEM solutions for $H(\text{grad})$ problem with parameters in (5.3) (e.g. $\alpha = 10^{-6}$) yielding a boundary layer.

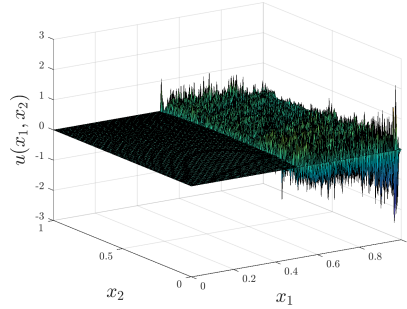
Next, we consider a similar problem on the same domain, with parameters,

$$(5.4) \quad \alpha(\mathbf{x}) = \begin{cases} 1, & x_1 < 0.5, \\ 10^{-6}, & x_1 \geq 0.5, \end{cases}, \quad \beta = \begin{bmatrix} 2 + x_1 \\ 1 + x_2 \end{bmatrix}, \quad \gamma = 0, \quad f = 1,$$

where the jump in the diffusion coefficient causes an internal layer.



(a) MFD solution of (3.16).



(b) Linear Lagrange FEM solution of (1.1).

Fig. 6: Comparison of MFD and FEM solutions for $H(\text{grad})$ problem with parameters in (5.4) (e.g. $\alpha = 1$ when $x_1 < 0.5$ and $\alpha = 10^{-6}$ when $x_1 \geq 0.5$) yielding an internal layer.

The solutions given by the MFD methods (solving (3.16)) with parameters given by (5.3) and (5.4) are plotted in Figure 5a and Figure 6a, respectively. It is clearly seen that there are no oscillations in the plots, and the jumps and layers are accurately captured. This demonstrates the monotonicity of the scheme. In contrast, both Figures 5b and 6b plot the solutions to the same boundary and internal layer problems but using a linear Lagrange FEM, which has large oscillations in the solution.

Remark 5.1. Though omitted for brevity, when (5.4) is modified to let

$$\alpha(\mathbf{x}) = \begin{cases} 10^6, & x_1 < 0.5, \\ 10^{-6}, & x_1 \geq 0.5, \end{cases},$$

the stability result still holds and yields a plot similar to Figure (6a). This is expected as the analysis is valid for the case where part of the domain is diffusion-dominated.

5.3. Boundary layer in $H(\text{curl})$. For the $H(\text{curl})$ problem, (1.2), we construct an example where a boundary layer is expected with the parameters,

$$(5.5) \quad \beta = \begin{bmatrix} 2 + x_1 \\ 1 + x_2 \end{bmatrix}, \quad \gamma = 1, \quad \mathbf{f} = \begin{bmatrix} 1 \\ 1 \end{bmatrix},$$

and varying α . The domain is again $\Omega = [0, 1] \times [0, 1]$ using a uniform mesh with $h = 1/64$. The values $\alpha = 10^{-1}$ and $\alpha = 10^{-6}$ are tested, and results are plotted in Figures 7 and 8. Again, the figure demonstrates that there are no spurious oscillations when using the MFD scheme. The boundary layer is accurately captured and the solution converges even as α varies by many orders of magnitude. In contrast, for

$\alpha = 10^{-1}$ we see almost exactly the same solution as MFD when using the lowest-order Nédélec finite elements. When α is reduced to 10^{-6} , the FEM solution is polluted with spurious oscillations.

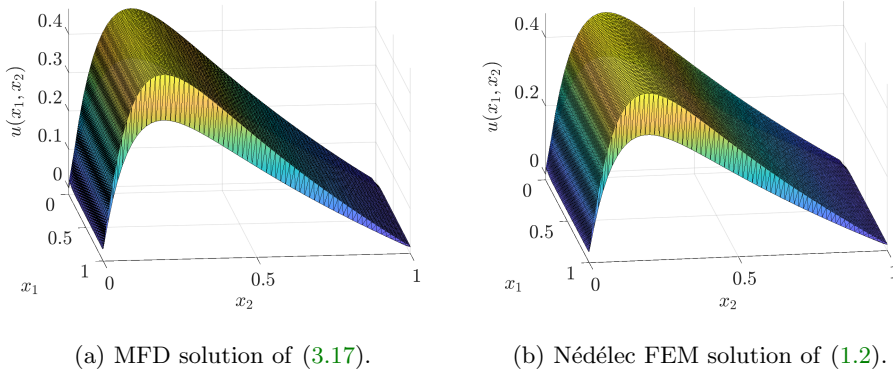


Fig. 7: Comparison of MFD and FEM solutions for $\mathbf{H}(\text{curl})$ problem with parameters in (5.5) and $\alpha = 10^{-1}$

5.4. Helmholtz Decomposition in $\mathbf{H}(\text{grad})$. Finally, we note that while our method relies on being able to write $\boldsymbol{\theta} = \boldsymbol{\beta}/\alpha$ in terms of a potential function, we do consider a way to handle the case where no such potential function exists, by using a Helmholtz decomposition, $\boldsymbol{\theta} = \text{grad } \varphi + \text{curl } \boldsymbol{\psi}$ (see Remark 3.1). Here, preliminary results are presented for the Helmholtz decomposition case for the scalar convection-diffusion equation. The tests given below are identical to the tests presented in (5.1) of Section 5.1, and (5.3) and (5.4) of Section 5.2, with the small modification of adding

$$(5.6) \quad \text{curl } \boldsymbol{\psi} = \text{curl} (.1 \sin(x_1 x_2))$$

to the convection parameter, $\boldsymbol{\beta}$. Figure 9 demonstrates that the convergence result holds even with the curl $\boldsymbol{\psi}$ added to the convection. From Figures 10a and 10b, we can see that monotonicity is preserved even with the modification to the convection coefficient.

6. Conclusions. This manuscript presented a stable MFD method for the general $\mathbf{H}(\mathfrak{D})$ convection-diffusion equation. The discrete flux operators allow for the convection-diffusion equations to be recast as a pure diffusion problem, and preserves the de Rham complex, guaranteeing that the method is structure-preserving regardless of the integration rule used to compute the exponential integrals. The MFD method can be thought of as a scaled, mass-lumped FE method. Using a FE framework allowed for a clear path for proving well-posedness via Babuška theory and deriving error estimates of the MFD scheme. Furthermore, the method is provably stable, meaning that as the diffusion coefficient tends to zero, $\alpha \rightarrow 0$, the discrete maximum principle or monotonicity property holds and the method will not suffer from numerical oscillations when the solution has shocks or boundary layers.

While only the lowest-order FE and MFD methods are studied here, higher-order methods [28, 46, 47, 64] require further investigation to see if a similar framework holds.

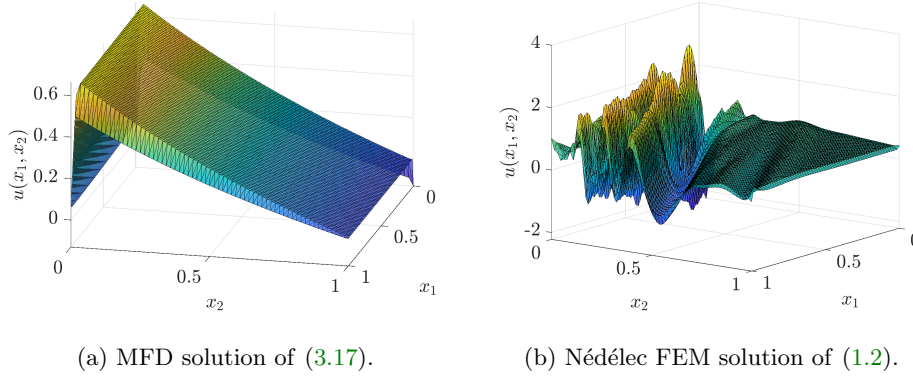


Fig. 8: Comparison of MFD and FEM solutions for $\mathbf{H}(\text{curl})$ problem with parameters in (5.5) and $\alpha = 10^{-6}$

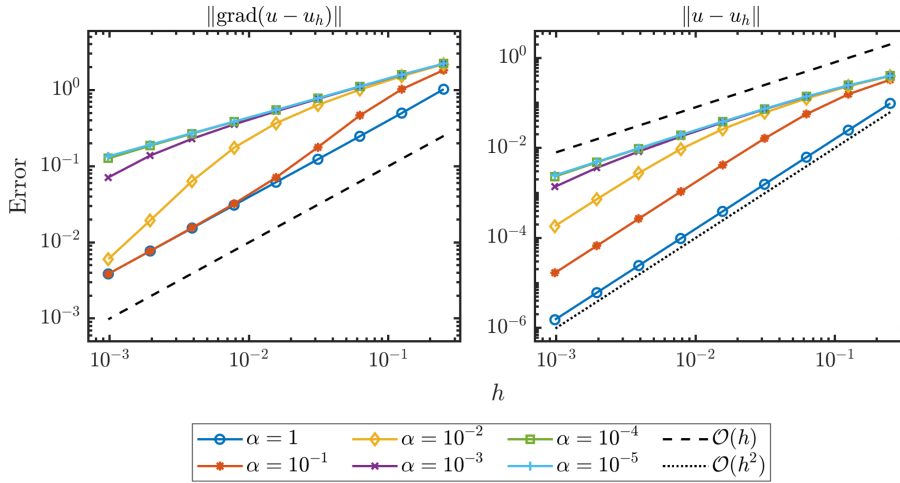
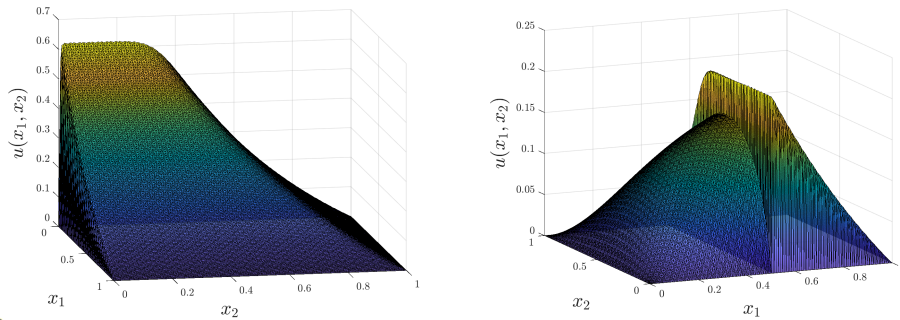


Fig. 9: MFD convergence results for modified (5.1), with error measured in $H(\text{grad})$ seminorm (left) and L^2 norm (right).

Additionally, since the flux operators satisfy a de Rham complex, iterative methods can be developed to efficiently solve the MFD system based on the FE theory. For instance, one could explore traditional multigrid methods for $H(\text{grad})$ and auxiliary space preconditioners for $\mathbf{H}(\text{curl})$ and $\mathbf{H}(\text{div})$. Some preliminary work has been done on this for the SAFE method, and those ideas could be extended to apply to MFD. Finally, we note that though the analysis presented only considers the case where $\boldsymbol{\theta} = \text{grad } \varphi$, we show results validating the stability when the coefficients can be represented by a Helmholtz decomposition, $\boldsymbol{\theta} = \text{grad } \varphi + \text{curl } \boldsymbol{\psi}$. Completing the analysis for this case requires further exploration.



(a) MFD solution to modified test (5.3). (b) MFD solution to modified test (5.4).

Fig. 10: MFD solutions to boundary layer and internal layer with Helmholtz decomposition for β in $H(\text{grad})$.

Acknowledgments. Sandia National Laboratories is a multimission laboratory managed and operated by National Technology and Engineering Solutions of Sandia, LLC, a wholly owned subsidiary of Honeywell International, Inc., for the U.S. Department of Energy’s National Nuclear Security Administration under contract DE-NA0003525. This paper describes objective technical results and analysis. Any subjective views or opinions that might be expressed in the paper do not necessarily represent the views of the U.S. Department of Energy or the United States Government.

N. Trask has been supported by the U.S. Department of Energy, Office of Advanced Scientific Computing Research under the U.S. Department of Energy, Office of Advanced Scientific Computing Research under the Early Career Research Program. A. Huang has been supported under the Sandia National Laboratories Laboratory Directed Research and Development (LDRD) program.

REFERENCES

- [1] J. H. ADLER, C. CAVANAUGH, X. HU, AND L. T. ZIKATANOV, *A finite-element framework for a mimetic finite-difference discretization of Maxwell’s equations*, SIAM J. Sci. Comput., 43 (2021), pp. A2638–A2659.
- [2] D. N. ARNOLD, *Finite element exterior calculus*, CBMS-NSF Regional Conference Series in Applied Mathematics, SIAM, 2018.
- [3] D. N. ARNOLD, R. S. FALK, AND R. WINTHER, *Finite element exterior calculus, homological techniques, and applications*, Acta Numer., 6 (2006), pp. 1–155.
- [4] B. AYUSO, R. HIPTMAIR, AND C. PAGLIANTINI, *Auxiliary space preconditioners for SIP-DG discretizations of $H(\text{curl})$ -elliptic problems with discontinuous coefficients*, IMA J. Numer. Anal., 37 (2017), pp. 646–686.
- [5] B. AYUSO, M. HOLST, Y. ZHU, AND L. ZIKATANOV, *Multilevel preconditioners for discontinuous Galerkin approximations of elliptic problems with jump coefficients*, Math. Comput., 83 (2014), pp. 1083–1120.
- [6] I. BABUŠKA, *Error-bounds for finite element method*, Numerische Mathematik, 16 (1971), pp. 322–333.
- [7] R. BANK, J. BÜRGER, W. FICHTNER, AND R. SMITH, *Some up-winding techniques for finite element approximations of convection diffusion equations*, Numer. Math., 58 (1990), pp. 185–202.
- [8] R. BANK AND D. ROSE, *Some error estimates for the box method*, SIAM J. Num. Anal., 24

- (1987), pp. 777–787.
- [9] R. BANK, P. VASSILEVSKI, AND L. T. ZIKATANOV, *Arbitrary dimension convection-diffusion schemes for space-time discretizations*, J. Comput. Appl. Math., 310 (2016).
 - [10] J. BARANGER, J. F. MAITRE, AND F. OUDIN, *Application de la théorie des éléments finis mixtes à l'étude d'une classe de schémas aux volumes différences finis pour les problèmes elliptiques*, C.R. Acad. ScL Paris, 319 (1994), pp. 401–404.
 - [11] ———, *Connection between finite volume and mixed finite element methods*, Modélisation mathématique et analyse numérique, 30 (1996), pp. 445–465.
 - [12] L. BEIRAO DA VEIGA, K. LIPNIKOV, AND G. MANZINI, *The mimetic finite difference method for elliptic problems*, Springer, 2014.
 - [13] A. BOSSAVIT, *Extrusion, contraction: their discretization via Whitney forms*, Int. J. Comput. Math. Elec. Elec. Engrg., 22 (2003), pp. 470–480.
 - [14] A. BOUSQUET, X. HU, M. S. METTI, AND J. XU, *Newton solvers for drift-diffusion and electrokinetic equations*, SIAM J. Sci. Comput., 40 (2018), pp. B982–B1006.
 - [15] N. BOZKAYA AND M. TEZER-SEZGIN, *Time-domain BEM solution of convection-diffusion-type MHD equations*, Int. J. Numer. Meth. Fluids, 56 (2008), pp. 1969–1991.
 - [16] F. BREZZI, M. FORTIN, AND L. D. MARINI, *Error analysis of piecewise constant pressure approximations of Darcy's law*, Comput. Methods Appl. Engrg., 195 (2006), pp. 1547–1559.
 - [17] F. BREZZI, L. P. FRANCA, AND A. RUSSO, *Further considerations on residual-free bubbles for advective-diffusive equations*, Comput. Methods Appl. Mech. Engrg., 166 (1998), pp. 25–33.
 - [18] F. BREZZI, D. MARINI, AND A. RUSSO, *Applications of the pseudo residual-free bubbles to the stabilization of convection-diffusion problems*, Comput. Methods Appl. Mech. Engrg., 166 (1998), pp. 51–63.
 - [19] F. BREZZI, L. D. MARINI, AND P. PIETRA, *Numerical simulation of semiconductor devices*, vol. 75, In Proceedings of the Eighth International Conference on Computing Methods in Applied Sciences and Engineering, 1987.
 - [20] F. BREZZI, L. D. MARINI, AND P. PIETRA, *Two-dimensional exponential fitting and applications to drift-diffusion models*, SIAM J. Numer. Anal., 26 (1989), pp. 1342–1355.
 - [21] F. BREZZI, L. D. MARINI, AND P. PIETRA, *Two-dimensional exponential fitting and applications to drift-diffusion models*, SIAM J. Numer. Anal., 26 (1989), pp. 1342–1355.
 - [22] F. BREZZI, L. D. MARINI, AND E. SULI, *Discontinuous Galerkin methods for first-order hyperbolic problems*, Math. Models Methods Appl. Sci., 14 (2004), pp. 1893–1903.
 - [23] F. BREZZI AND A. RUSSO, *Choosing bubbles for advection-diffusion problems*, Math. Models Methods Appl. Sci., 4 (1994), pp. 571–587.
 - [24] A. N. BROOKS AND T. J. HUGHES, *Streamline upwind/Petrov-Galerkin formulations for convection dominated flows with particular emphasis on the incompressible Navier–Stokes equations*, Comput. Methods Appl. Mech. Engrg., 32 (1982), pp. 199–259.
 - [25] E. BURMAN, *A unified analysis for conforming and nonconforming stabilized finite element methods using interior penalty*, SIAM J. Numer. Anal., 43 (2005), pp. 2012–2033.
 - [26] ———, *Consistent SUPG-method for transient transport problems: stability and convergence*, Comput. Methods Appl. Mech. Engrg., 199 (2010), pp. 1114–1123.
 - [27] E. BURMAN AND A. ERN, *Continuous interior penalty hp-finite element methods for advection and advection-diffusion equations*, Math. Comp., 76 (2007), pp. 1119–1140.
 - [28] J.E. CASTILLO, J.M. HYMAN, M.J. SHASHKOV, AND S. STEINBERG, *High-order mimetic finite difference methods on nonuniform grids*, Houston J. Math, Special Issue (1995), pp. 347–361.
 - [29] C. CAVANAUGH, *Structure-Preserving Discretizations for Partial Differential Equations*, PhD thesis, Tufts University, 2022. <https://dl.tufts.edu/concern/pdfs/mk61rx87s>.
 - [30] S. H. CHRISTIANSEN, T. G. HALVORSEN, AND T. M. SØRENSEN, *Stability of an upwind Petrov–Galerkin discretization of convection diffusion equations*, preprint, (2014). <https://arxiv.org/abs/1406.0390>.
 - [31] P. DEGOND AND S. MAS-GALLIC, *The weighted particle method for convection-diffusion equations. part 1: The case of an isotropic viscosity*, Math. Comput., 53 (1989), pp. 485–507.
 - [32] W. DÖRFLER, *Uniform error estimates for an exponentially fitted finite element method for singularly perturbed elliptic equations*, SIAM J. Numer. Anal., 36 (1999), pp. 1709–1738.
 - [33] L. C. EVANS, *Partial differential equations*, American Mathematical Society, 2010.
 - [34] L. P. FRANCA AND L. TOBISKA, *Stability of the residual free bubble method for bilinear finite elements on rectangular grids*, IMA J. Numer. Anal., 22 (2002), pp. 73–87.
 - [35] J.-F. GERBEAU, C. LE BRIS, AND T. LELIEVRE, *Mathematical methods for the magnetohydrodynamics of liquid metals*, Clarendon Press, 2006.
 - [36] H. HEUMANN AND R. HIPTMAIR, *Eulerian and semi-Lagrangian methods for convection-diffusion for differential forms*, Discrete Contin. Dyn. Syst., 29 (2011), pp. 1497–1516.

- [37] H. HEUMANN, R. HIPTMAIR, AND C. PAGLIANTINI, *Stabilized galerkin for transient advection of differential forms*, Discrete Cont. Dyn-S, 9 (2015).
- [38] R. HIPTMAIR, *Finite elements in computational electromagnetism*, Acta Numer., 11 (2002), pp. 237–339.
- [39] P. HOUSTON, C. SCHWAB, AND E. SULI, *Discontinuous hp-finite element methods for advection-diffusion-reaction problems*, SIAM J. Numer. Anal., 39 (2002), pp. 2133–2163.
- [40] P. HSIEH AND S. YANG, *Two new upwind difference schemes for a coupled system of convection-diffusion equations arising from the steady MHD duct flow problems*, J. Comput. Phys., 229 (2010), pp. 9216–9234.
- [41] S. B. JI, A. G. GERBER, AND A. C. SOUSA, *A convection-diffusion CFD model for aeolian particle transport*, Int. J. Numer. Meth. Fluids, 45 (2004), pp. 797–817.
- [42] R. LAZAROV AND L. T. ZIKATANOV, *An exponential fitting scheme for general convection-diffusion equations on tetrahedral meshes*, Appl. Math. Comput., 92 (2012).
- [43] R. D. LAZAROV AND L. T. ZIKATANOV, *An exponential fitting scheme for general convection-diffusion equations on tetrahedral meshes*, Comput. Appl. Math., 1 (2012), pp. 60–69.
- [44] S. LEE, *Edge-averaged virtual element methods for convection-diffusion equations*, PhD thesis, University of California, Irvine, 2021.
- [45] G. LEONARD, M. MITCHNER, AND S.A. SELF, *Particle transport in electrostatic precipitators*, Atmos. Environ., 14 (1980), pp. 1289–1299.
- [46] K. LIPNIKOV AND V. GYRYA, *High-order mimetic finite difference method for diffusion problems on polygonal meshes*, J. Comput. Phys., 227 (2008), pp. 8841–8854.
- [47] K. LIPNIKOV, G. MANZINI, AND M. SHASHKOV, *Mimetic finite difference method*, J. Comput. Phys., (2013).
- [48] ———, *Mimetic finite difference method*, J. Comput. Phys., 257 (2014), pp. 1163–1227.
- [49] M. S. METTI, J. XU, AND C. LIU, *Energetically stable discretizations for charge transport and electrokinetic models*, J. Comput. Phys., 306 (2016), pp. 1–18.
- [50] K.W. MORTON, *Numerical Solution of Convection-Diffusion Problems*, CRC Press, 1st ed. ed., 1996.
- [51] K. W. MORTON, *The convection-diffusion Petrov–Galerkin story*, IMA J. Numer. Anal., 30 (2009), pp. 231–240.
- [52] R. J. PLEMMONS, *M-matrix characterizations. I–nonsingular M-matrices*, Linear Algebra Appl., 18 (1977), pp. 175–188.
- [53] C. RODRIGO, F. J. GASPAR, X. HU, AND L. T. ZIKATANOV, *Finite element framework for some mimetic finite difference discretizations*, Comput. Math. Appl., 70 (2015), pp. 2661–2673.
- [54] D. SCHARFETTER AND H. GUMMEL, *Large-signal analysis of a silicon read diode oscillator*, IEEE Trans. Electron Devices, 205 (1969), pp. 959–962.
- [55] T. W. H. SHEU, K. C. LIN, AND J. H. LI, *Development of a convection-diffusion-reaction model for solving Maxwell’s equations in frequency domain*, Int. J. Numer. Meth. Fluids, 69 (2012), pp. 430–441.
- [56] T. W. H. SHEU AND R. K. LIN, *Development of a convection-diffusion-reaction magnetohydrodynamics solver on non-staggered grids*, Int. J. Numer. Meth. Fluids, 45 (2004), pp. 1209–1233.
- [57] O. SHIPILOVA, H. HAARIO, AND A. SMOLIANSKI, *Particle transport method for convection problems with reaction and diffusion*, Int. J. Numer. Meth. Fluids, 54 (2007), pp. 1215–1238.
- [58] G. STRANG, *Variational crimes in the finite element method*, in The mathematical foundations of the finite element method with applications to partial differential equations, Elsevier, 1972, pp. 689–710.
- [59] V. THOMÉE, *Galerkin finite element methods for parabolic problem*, Springer, 1997.
- [60] N. TRASK, A. HUANG, AND X. HU, *Enforcing exact physics in scientific machine learning: a data-driven exterior calculus on graphs*, J. Comput. Phys., 456 (2022), p. 110969.
- [61] P. N. VABISHCHEVICH, *Finite-difference approximation of mathematical physics problems on irregular grids*, Comput. Methods Appl. Math., 5 (2005), pp. 294–330.
- [62] D. WALTER, H. FICHTNER, AND Y. LITVINENKO, *A perturbative approach to a nonlinear advection-diffusion equation of particle transport*, Phys. Plasmas, 27 (2020), p. 82901.
- [63] S. WU AND J. XU, *Simplex-averaged finite element methods for $H(\text{grad})$, $H(\text{curl})$, $H(\text{div})$ convection-diffusion problems*, SIAM J. Numer. Anal., 58 (2020), pp. 884–906.
- [64] S. WU AND L. T. ZIKATANOV, *On the unisolvence for the quasi-polynomial spaces of differential forms*, preprint, (2020). <https://arxiv.org/abs/2003.14278>.
- [65] L. T. ZIKATANOV AND J. XU, *A monotone finite element scheme for convection-diffusion equations*, Math. Comp., 68 (1999), pp. 1429–1446.